University of Stavanger

Faculty of Science and Technology

MASTER'S THESIS

Study program/Specialization: Petroleum Engineering/Reservoir Engineering	Spring semester, 2011 Open Access
Writer: Eko Yudhi Purwanto	
Faculty supervisor: SveinSkjæveland External supervisor(s): Ingebret Fjelde and Arield Lohne	
Titel of thesis: Effect of IFT on Gravity Segregation in Mixed Wet Reservoir	
Credits (ECTS): 30	
Key words: Mixed Wettability Gravity Segregation IFT Surfactant Flooding ECLIPSE Surfactant Model	Pages: 53 + enclosure: 14 Stavanger, 15 June 2011

Frontpage for master thesis
Faculty of Science and Technology
Decision made by the Dean October 30th 2009

ACKNOWLEDGEMENT

Even though this master thesis is an independent work, a lot of people have helped me in some ways throughout the work.

I owe my deepest gratitude to Ingebret Fjelde for providing me facilities, guidance, and advices to improve the quality of this thesis.

Arield Lohne, who shared so much valuable knowledge with me, is the other one I want to acknowledge especially. Many parts of this thesis arise from our long discussions. His views are always illuminating.

I also want to acknowledge Edwin for providing me invaluable help with Eclipse in the beginning phase of this work.

I also owe a special acknowledgement to Svein Skjæveland, who gave me a very useful book and reviewed the draft of this thesis even during the weekend.

Finally, I am grateful to University of Stavanger (UiS) and International Research Institute of Stavanger (IRIS) as the institutions that gave me the opportunity to perform this work.

Last but not least, thank you to my wife, Trimaharika Widarena, for her continuous support that always makes me stronger.

ABSTRACT

The effects of water-oil interfacial tension (IFT) on gravity segregation and its implication on oil recovery have been investigated by numerical simulations and steady state upscaling. Eclipse surfactant model was used to introduce the reduction of IFT. Micro-scale mechanisms of the surfactant model, such as relative permeability alteration and residual oil saturation (S_{or}) reduction, were turned off in order to isolate the effect of IFT on gravity segregation mechanism.

Oil recovery in the system with gravity segregation was found to be higher than the oil recovery given by the system without gravity segregation. Gravity segregation behind the displacement front caused the oil phase to move upwards and eventually accumulated at the top of the model, thus increasing the effective horizontal oil mobility. Capillary forces will act against this segregation. A reduction in IFT will decrease the capillary forces, thus increasing magnitude of the segregation.

The degree of gravity segregation was also found to increase with increasing water-oil density difference, increasing model thickness, and increasing horizontal permeability. A correlation between the degree of gravity segregation and dimensionless Bond number (N_B) which combines all of those parameters was established. If the N_B is plotted against the S_{or}, the shape of the curve would resemble the Capillary Desaturation Curve (CDC) in which there is a critical value where the S_{or} starts to decrease.

Gravity segregation is a slow process. Low injection velocity must be applied in order to give sufficient time for the gravity forces to act in the system. There is a critical velocity above which gravity segregation will not be observed. This critical velocity was found to increase with increasing vertical permeability, increasing oil-water density difference, and decreasing the model thickness. All of the pertinent parameters were then combined in the form of dimensionless viscous-gravity ratio (R_{vg}). It was found that gravity segregation will start to occur when the R_{vg} equals to one.

TABLE OF CONTENTS

LIST OF FIGURES

LIST OF TABLES

NOMENCLATURE

μ	= Viscosity
1D	= One-dimensional
2D	= Two-dimensional
A	= Cross sectional area
ASP	= Alkaline/Surfactant/Polymer
CDC	= Capillary Desaturation Curve
CMC	= Critical Micelles Concentration
C_{Surf}	= Surfactant concentration
E	= Overall displacement efficiency
E_d	= Microscopic displacement efficiency
EOR	= Enhanced Oil Recovery
E_v	= Macroscopic/volumetric displacement efficiency
FVF	= Formation Volume Factor
g	= Gravitational constant
H	= Thickness
IFT	= Interfacial Tension
IOIP	= Initial Oil in Place
J	= Dimensionless capillary pressure
k	= Absolute permeability
k_h	= Horizontal permeability
k_{ro}	= Relative permeability to oil
k_{rw}	= Relative permeability to water
k_v	= Vertical permeability
L	= Length
M	= Mobility ratio
N_B	= Bond number
N_C	= Capillary number
Ø	= Porosity
P_C	= Capillary pressure
PV	= Pore Volume
r	= Radius of capillary
ROS	= Remaining Oil Saturation
R_{vg}	= Viscous-gravity forces ratio
S	= Saturation

S_{of}	= Final oil saturation
S_{or}	= Residual oil saturation
Subscript d	= Displaced fluid
Subscript D	= Displacing fluid
Subscript o	= Oil
Subscript w	= Water
VE	= Vertical equilibrium
WBHP-I	= Well bottomhole pressure of the injection well
WBHP-P	= Well bottomhole pressure of the production well
WCF	= Well connection factor
Δp	= Pressure drop
Δx	= Grid block size in x direction
θ	= Contact angle
ρ	= Density

1 INTRODUCTION

1.1 Background

In this modern global economy, we cannot live without energy and most of the energy supply comes from petroleum fuel. **Figure 1.1** shows historical energy consumption in the United States taken from U.S. Energy Information Administration, EIA (2011). It can be seen that petroleum has been the major contributor to the energy consumption for the latter half of the 20th century.

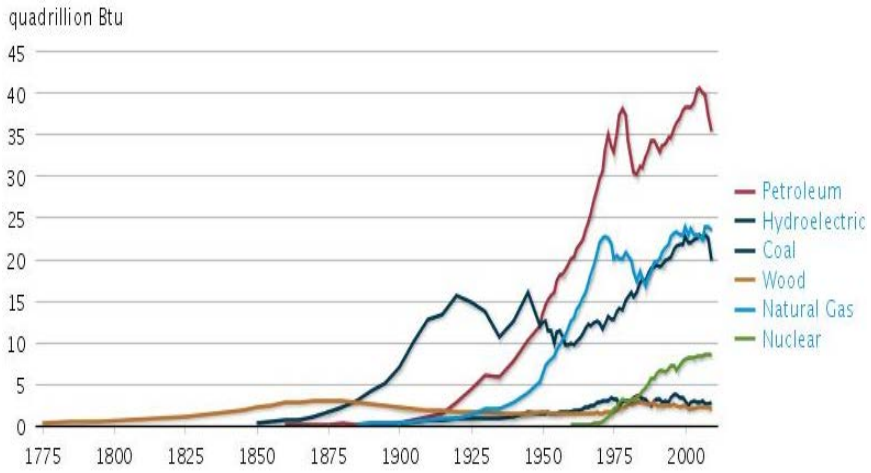

Figure 1.1 History of energy consumption in the United States (EIA, 2011).

As the world population continuously grows, the demand of energy is expected to increase in the coming years. **Figure 1.2** provides historical data and projection of the world energy consumption from 1990 to 2035. According to the EIA (2011), the world energy consumption will on average continue to increase by 2% per year and it leads to a doubling of the energy consumption every 35 years. Therefore, continuous increase of energy supply is important in order to be able to balance the demand.

Energy diversification is perhaps the best solution to overcome this situation. In addition to that, Enhanced Oil Recovery (EOR) could also be an important effort to increase the energy supply. According to Green and Willhite (1998), conventional methods of oil production produce only about one-third of the initial oil in place (IOIP) and the rest remains in the reservoir. Properly designed and executed EOR projects are expected to be able to recover some of the remaining oil by improving the displacement efficiency.

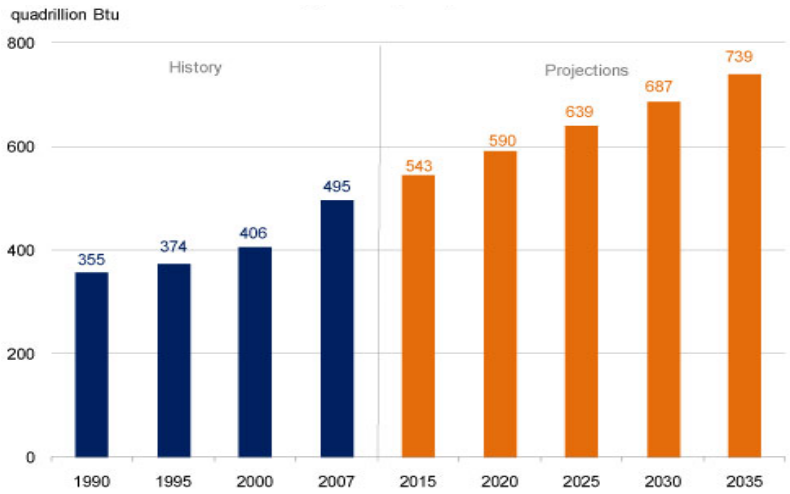

Figure 1.2 World energy consumption from 1990 to 2035 (EIA, 2011).

Surfactant flooding is one of the common EOR methods in which surfactant solution is added into the injection water. Surfactants reduce interfacial tension (IFT) between oil and water phase (Ottewill, 1984). As the IFT is reduced, the ability of the water phase to displace the trapped oil phase increases and thereby increasing the oil recovery.

Surfactant flooding requires substantial initial cost for chemicals. When the oil price was low, this high initial cost became a prohibitive factor for research in surfactant flooding. However, with the current higher oil price, it seems reasonable to perform a study on surfactant flooding for enhancing our understanding about its mechanism.

1.2 Objectives

According to Melrose and Brandner (1974), a reduction in IFT might decrease the residual oil saturation (S_{or}). It is generally recognized as the main oil recovery mechanism in surfactant flooding. Some authors also reported that a reduction in IFT will also enhance the fluids segregation due to the gravity forces (Hornof and Morrow, 1987). This gravity segregation at the displacement front is normally considered as a negative effect in a displacement process because it causes the injected fluid to over-ride or under-ride the reservoir oil, thus bypassing the oil at the bottom or top of the reservoir.

However, gravity segregation acting behind the displacement front might result in different effects. This study was intended to investigate the mechanism of gravity segregation behind the displacement front and its implication on oil recovery. The mechanism was investigated by means of numerical simulation experiments. A set of saturation functions taken from

mixed wet core was used in all of the simulations. The ultimate goals of this work were to study the effect of water-oil IFT reduction on gravity segregation in various conditions and to find correlations between the behavior of gravity segregation and rock-fluids properties.

This master thesis is divided into six chapters. In Chapter 1, introduction and objectives of the study are presented. Chapter 2 and 3 summarize previous studies related to wettability and surfactant flooding. The methodology carried out in this study, along with the results and discussions are provided in Chapter 4 and 5. Chapter 6 contains the conclusions and recommendations for further work.

2 MIXED WETTABILITY

2.1 Introduction

Wettability is the tendency of one fluid to spread on a solid surface in a multiphase fluids system (Green and Willhite, 1998). When two immiscible fluids are in contact with a solid surface, one fluid tends to be attracted to the solid more strongly than the other fluid. The more strongly attracted fluid is called the wetting fluid.

Wettability is a major factor controlling the distribution of fluids in a porous medium. Donaldson and Thomas (1971) reported that the wetting phase tends to occupy the small pores and forms a thin film over all the rock surfaces because of the attractive forces between the wetting phase and the rock surfaces, while the non-wetting phase is located in the center of the larger pores.

A water wet rock will preferentially contact water while an oil wet rock will preferentially contact oil. Reservoir rocks are also known to have intermediate or neutral wettability in which both oil and water phase tend to wet the solid. The classification of reservoirs as water wet, oil wet, or intermediate wet is a rough simplification. Anderson (1987a) reported that reservoir wettability can cover broad range of wetting condition that varies from very strongly water wet to very strongly oil wet, complex wettability conditions given by combinations of water wet and oil wet surfaces have also been identified.

According to Cosentino (2001), as all reservoir rocks were originally deposited in an aqueous environment, the water molecules were therefore promptly adsorbed onto the grain surfaces during sedimentation. Consequently, all reservoir rocks started out as water wet. During and after oil accumulation, the oil molecules might displace some of the water molecules from the surface film. Depending on whether the water molecules are partly or totally displaced in this way, the rock might acquire partial wettability to oil, or become totally oil wet.

In the early days of petroleum engineering, it was a common practice to assume that oil reservoirs were strongly water wet due to the fact that water originally occupied the reservoir (Cosentino, 2001). However, Anderson (1987b) reported that many reservoir rocks exhibit non uniform wettability, whereby the rocks contain both water wet and oil wet fractions. Agbalaka et al. (2008) even suggested that non uniform wettability might be the normal condition in the reservoir.

Non uniform wettability can be further divided into two categories: fractional wettability and mixed wettability. A reservoir is called fractionally wet if oil wet and water wet rocks are packed in different parts of the rock. Mixed wettability was first introduced by Salathiel (1973) to describe systems where the larger pores are oil wet, and the smaller pores remain water wet. Such situations may arise when oil migrates to water wet reservoirs and preferentially fills the larger pores. The wettability of these larger pores may then be altered to oil wet by deposition of organic matter from the oil.

Wettability can be expressed conveniently by measuring the angle of contact at the liquid-solid surface. This angle, which is normally measured through the water phase, is called contact angle. As shown in **Figure 2.1**, a solid is water wet if the contact angle is less than 90^o, and oil wet if it is more than 90^o. Intermediate wet is identified when the contact angle is close to 90^o.

Apart from the contact angle measurement, several types of laboratory experiments for determining wettability have been described in the literatures as reported by Anderson (1986). One of the common methods is USBM (U.S. Bureau of Mines) which employs the wettability index to express the wettability preferences of a core. In particular, a wettability index equals to 0 indicates an intermediate wet, while value of +1 and -1 indicate strongly water wet and strongly oil wet, respectively. Wettability index represents the average wettability of a core, while the contact angle measures the wettability of a specific surface.

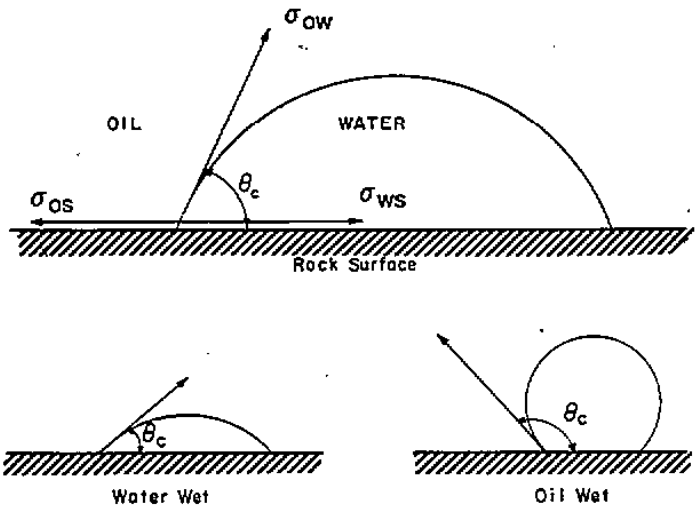

Figure 2.1 Determining wettability from contact angle (Raza et al., 1968).

2.1 Effect of Wettability on Relative Permeability

Rao et al. (1992) measured oil-water relative permeabilities from four rock-fluids systems with different wettability preferences. The data obtained are presented in **Figure 2.2**. The water wet characteristic of Beaverhill Lake (BL) rock-fluids is identified in which the end point oil permeability is high (about 95% of the absolute permeability) and the end point water permeability is low (about 10% of the absolute permeability). In contrast, the Crossfield Cardium (CC) rock-fluids system clearly shows oil wet nature in which the end point water permeability is much higher than the end point oil permeability.

The relative permeability curves for the Gilwood (GW) rock-fluids system indicate an intermediate wet since the end point oil permeability is only about 30% of the absolute permeability while the end point water permeability is almost 20% of the absolute. The relative permeability curves for the Gilwood fluid – Berea (GB) system are comparable to those of the intermediate wet GW system. However, the saturation band covered by water permeability for the GB system is somewhat larger than that for the intermediate wet GW system. Despite similar relative permeability characteristics, the authors found that the GB system yielded significantly higher oil recoveries than in the intermediately wet GW system. Therefore, the GB system is considered to be a mixed wet.

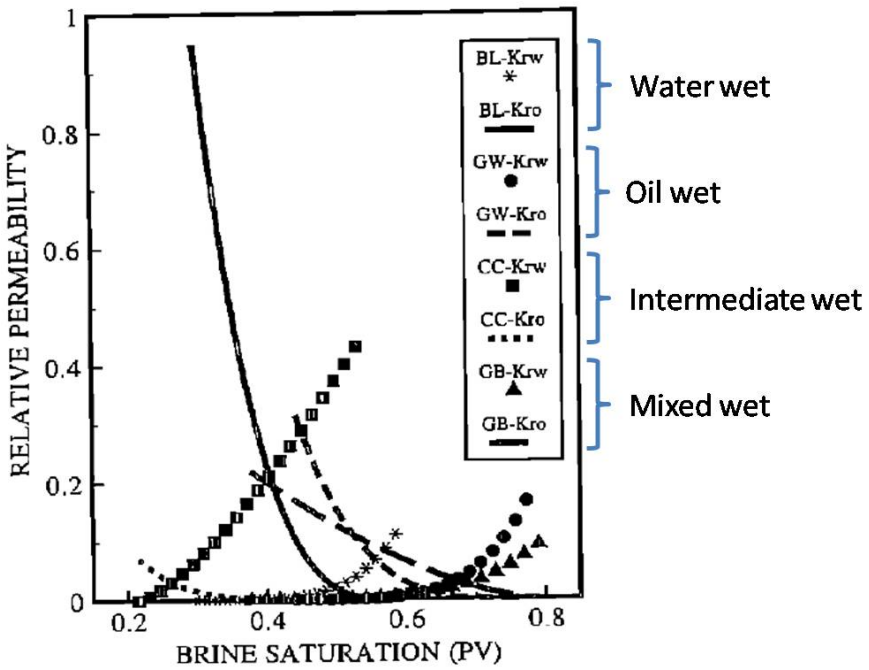

Figure 2.2 Oil-water relative permeability in various wettability preferences (Rao et al., 1992).

According to Raza et al. (1968), the end point water permeability is lower in the water wet system when compared with the oil wet system because the residual oil in the water wet is trapped as discontinuous droplets in the larger pores. These droplets block pore throats, thus lowering the water permeability. On the other hand, the residual oil in the oil wet system is located in the smaller pores and as film on the solid surfaces, where it has little effect on the water flow.

2.2 Effect of Wettability on Capillary Pressure

Behbahani and Blunt (2004) performed an analysis of imbibition processes in mixed wet rocks using pore scale modeling. Berea cores were saturated with Prudhoe Bay crude oil. Then the samples were aged for between 0 and 240 hours to alter the wettability of the samples from water wet towards mixed wettability. The capillary pressures from each sample were measured and the results are shown in **Figure 2.3**. As the samples become more mixed wet, the capillary pressure becomes lower and an increasing fraction of the curve lies below zero, indicating oil wet properties. The capillary pressures above zero represent the process when the samples imbibed water, while those below zero represent the process when the samples imbibed oil. These results show that the mixed wet cores have the ability to imbibe both water and oil.

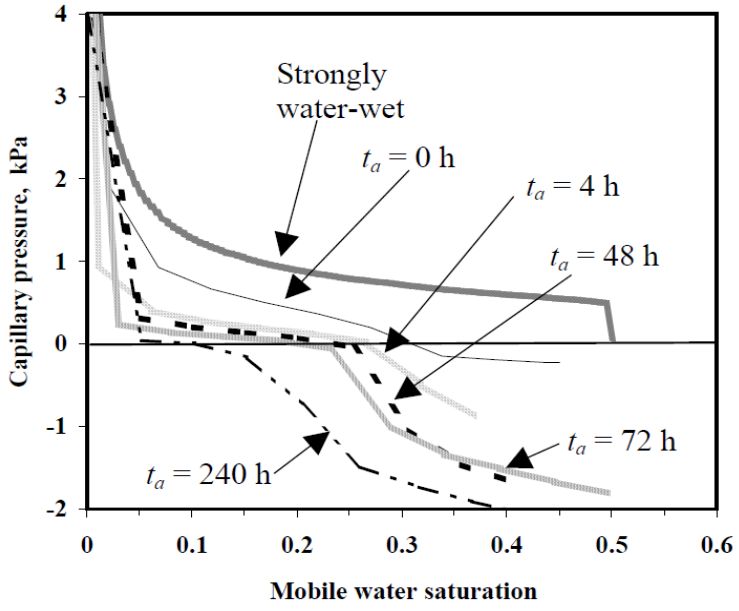

Figure 2.3 Capillary pressure for different wettability states as represented by aging times, t_a (Behbahani and Blunt, 2004).

2.3 Effect of Wettability on Oil Recovery

Raza et al. (1968) described the process of waterflooding in water wet and oil wet system as illustrated in **Figure 2.4**. Water displacing oil from a water wet pore is shown in **Figure 2.4a**. The rock surface is preferentially wetted by the water, so water will move forward along the pores wall, displacing oil in front of it. At some point, the remaining oil will become disconnected, leaving an oil droplet trapped in the center of the pore. After the water front passes, most of the remaining oil is immobile. Because of such immobility in this water wet case, there is little or no oil production after water breakthrough.

Oil displacement process in an oil wet system is illustrated in **Figure 2.4b**. When the waterflooding is started, the water will form continuous channels through the centers of the larger pores, displacing oil in front of it. Oil is left in the smaller pores and as a continuous film over the pore surfaces. Because much of the remaining oil is still continuous, additional oil can be produced after water breakthrough. There is a tendency for the water to finger through the larger pores and bypassing the oil in the smaller pores, thus earlier water breakthrough is normally observed in an oil wet system. It is generally accepted that waterflooding is less efficient in oil wet systems compared with water wet ones because of earlier water breakthrough and more water must be injected to recover a given amount of oil.

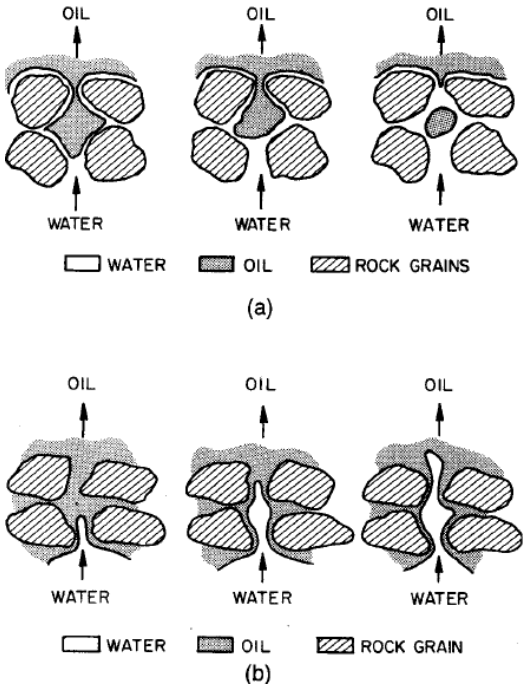

Figure 2.4 Oil displacement process in (a) water wet and (b) oil wet system (Raza et al., 1968).

Salathiel (1973) compared waterflooding performance first in water wet core, and then in the same core rendered mixed wettability. ROS (Remaining Oil Saturation) as a function of PV (Pore Volume) injected is presented in **Figure 2.5**. As expected, there is very little or no oil production after water breakthrough when the core is water wet. The final oil saturation is about 35%. In the mixed wet core, more oil is recovered after the injection of the same amount of water. The oil saturation keeps decreasing as long as the water is injected; indicating small but finite oil permeability exists even at very low oil saturation. Very low residual oil saturation (~10%) will be achieved by injection of many PV of water. The author postulated that the very low residual oil saturation is obtained because of surface film drainage mechanism.

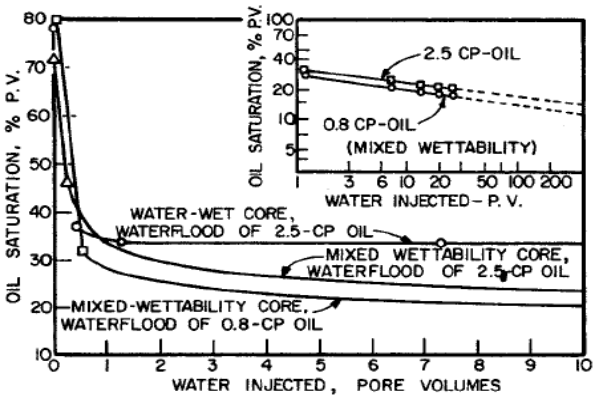

Figure 2.5 Comparison of waterflooding behaviour in mixed-wet and water-wet cores (insert shows extension of mixed wettability flooding data) (Salathiel, 1973).

Laboratory experiments done by Salathiel (1973) also demonstrated that the surface film drainage of oil depends on the composition of the reservoir fluids and rock properties. Therefore, the process does not occur in all mixed wet reservoirs. In those mixed wet reservoirs where surface film drainage can occur, very low residual oil saturation can only be achieved if depletion times are long enough for gravity segregation to be effective.

Wood et al. (1991) measured residual oil saturation in Endicott core sample, which possesses typical mixed wettability characteristic. They showed that the remaining oil saturation is a strong function of PV injected. After 1 PV injection, the ROS is 40%, whereas after 500 PV the oil saturation is 22% and still falling. In addition, they also found that high vertical permeability is essential for surface film drainage to be effective. These results reveal that gravity segregation is an important oil recovery mechanism in mixed wet system.

3 SURFACTANT FLOODING

3.1 Introduction

Based on the process description, Green and Willhite (1998) divided oil recovery processes into primary, secondary, and EOR process. Primary recovery is the recovery of oil by any of the natural energy sources present in a reservoir without supplementary help from injected fluids. These natural energy sources could be natural water drive, solution gas drive, gas cap drive, fluid and rock expansion, or gravity drainage.

Secondary recovery uses additional energy from injection of water or gas to displace oil toward producing wells (Lake, 1989). Water or gas is either injected into water or gas zone for pressure maintenance or injected into oil zone to displace oil immiscibly according to volumetric sweepout considerations. Waterflooding is perhaps the most common method of secondary recovery.

Lake (1989) defined EOR as oil recovery by means of injection of materials not normally present in reservoir. The injected fluids supplement the natural energy in the reservoir to displace oil to a producing well. These processes differ from secondary recovery in such a way that the injected fluids interact with the reservoir rock/oil system to create favorable condition for oil recovery. These interactions include lower water-oil IFT, oil swelling, oil viscosity reduction, wettability alteration, or favorable phase behavior.

Typically, a reservoir will undergo primary production followed by waterflooding (Green and Willhite, 1998). Recovery by those processes might approach 35 to 50% IOIP when the waterflooding reaches an economic limit. The remaining oil in the reservoir is a large and attractive target for EOR methods. However, EOR is not necessarily applied in the last stage of production. In some cases, EOR is applied as the initial stage of production. The usual situation is viscous oil that would not be produced economically by primary mechanism or waterflooding. In other cases, EOR might be applied after primary production (as a second stage production).

Kate Van Dyke (1997) subdivided EOR techniques into three main categories; thermal recovery, miscible injection, and chemical injection.

- Thermal recovery

  This technique is intended to reduce the viscosity of heavy oil by applying heat, thus improving the mobility and allowing the oil to be displaced to the producers. This is

the most common EOR technique. Hot water or steam drive, steam soak, and in situ combustion are several methods for generating the heat.

- Miscible injection

  Miscible injection is aimed to recover residual oil by using a displacing fluid which mixes with oil in the reservoir. Typical miscible drive fluids include hydrocarbon solvents, hydrocarbon gases, and carbon dioxide. Because those fluids are usually more mobile than oil, they tend to bypass the oil resulting in low displacement efficiency. This method is therefore best suited to high dip reservoirs.

- Chemical flooding

  Chemical flooding involves the addition of one or more chemical compounds to the injected water to improve displacement efficiency by either reducing water-oil IFT or increasing the injected water viscosity, makes it less likely to bypass the oil. Surfactant, polymer, and alkaline are among the chemicals used in chemical flooding.

3.2 Surfactants

Surfactant is a surface active agent that contains a hydrophobic (dislikes water) and a hydrophilic (likes water) part as schematically illustrated in **Figure 3.1**, taken from Ottewill (1984). The hydrophobic portion is often called the tail and the hydrophilic portion the head of the molecule.

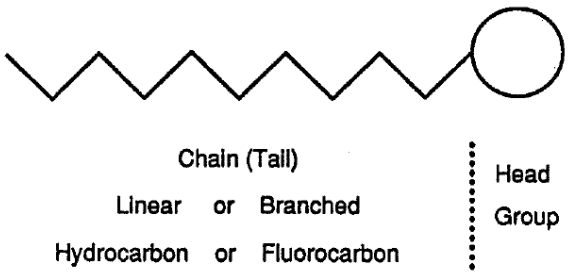

Figure 3.1 Schematic of surfactant molecule (Ottewill, 1984).

When surfactant is added into water-oil system at low concentration, the dissolved surfactant molecules are dispersed as monomers and migrate to the interface between the oil and water phase. As the surfactant concentration is increased, the surfactant molecules start to form

aggregates or micelles in a very narrow range of concentration called Critical Micelle Concentration (CMC). Further increase of surfactant concentration results in the formation of more micelles but relatively small change in monomer concentration. **Figure 3.2** shows water-oil system with surfactant concentration above CMC. The monomers reside at the water-oil interface while the micelles are located either in the oil or water phase.

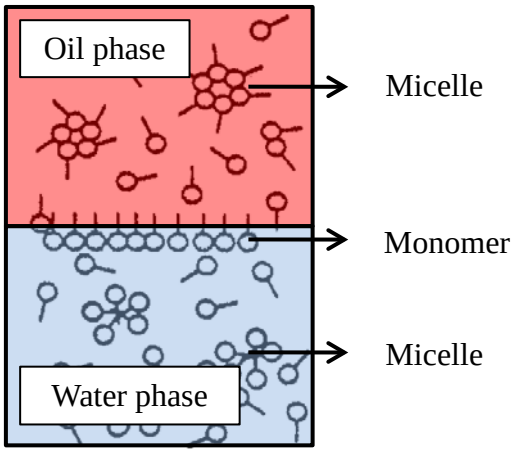

Figure 3.2 Water-oil system with surfactant concentration above CMC (Green and Willhite, 1998).

Water-oil IFT is a strong function of the surfactant's monomers concentration. **Figure 3.3** illustrates the general behavior of IFT as a function of surfactant concentration. The IFT decreases significantly as surfactant concentration increases until the CMC is reached. Surfactant added in excess of the CMC will not increase the concentration of monomers at the water-oil interface, thus little change in water-oil IFT occurs.

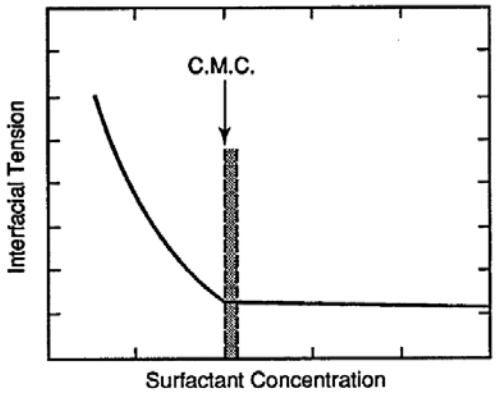

Figure 3.3 IFT as a function of surfactant concentration (Green and Willhite, 1998).

3.3 Displacement Process

Craft and Hawkins (1991) defined the overall displacement efficiency (E) of any oil displacement process as a product of volumetric (E_v) and microscopic displacement efficiency (E_d). In the form of equation, it can be expressed as follow:

$$E = E_v \times E_d \tag{3.1}$$

The volumetric displacement efficiency refers to the effectiveness of the displacing fluid in contacting the reservoir. It is governed by areal and vertical displacement efficiency. Both of those efficiencies can be improved by maintaining favorable mobility ratio (M) throughout the process.

$$M = \frac{\left(k_r/\mu\right)_D}{\left(k_r/\mu\right)_d} \tag{3.2}$$

Where k_r = relative permeability, μ = viscosity, subscript D and d = displacing and displaced fluid, respectively. Favorable mobility ratio is achieved when the mobility of the displacing fluid is lower than the mobility of the displaced fluid. In such situation, it is less likely for the displacing fluid to bypass the displaced fluid. Polymer flooding is intended to decrease mobility of the displacing fluid by increasing its viscosity.

The vertical displacement efficiency is affected by the density difference between the displacing and displaced fluid. Large density difference can result in gravity segregation. Gravity segregation at the displacement front is generally considered as a negative effect on displacement efficiency. The effect is to bypass fluids at the top (under-riding) or bottom (over-riding) of the reservoir, reducing the displacement efficiency in vertical cross section. The vertical displacement efficiency is also affected by vertical permeability variation. In a layered reservoir with vertical variation in permeability, the displacing fluid tends to flow in

the layer with the greatest permeability which leads to an uneven flow in different layers, thus reducing vertical displacement efficiency.

The microscopic displacement efficiency refers to the effectiveness of the displacing fluid in mobilizing the oil in the swept region. It is expressed in the magnitude of the residual oil saturation (S_{or}) in the regions contacted by the displacing fluid. The microscopic displacement efficiency can be improved by increasing the capillary number (N_c), a dimensionless ratio between viscous and capillary forces. There are numerous alternatives to express the capillary number. The following equations are some of the commonly used expressions.

$$N_c = \frac{u \times \mu}{IFT} = \frac{\Delta p \times k_h}{L \times IFT} \tag{3.3}$$

Where u = velocity, μ = viscosity, Δp = pressure drop, k_h = horizontal permeability, L = length, and IFT = interfacial tension between oil and water.

The relationship between the capillary number and residual oil saturation is commonly called Capillary Desaturation Curve (CDC). **Figure 3.4** shows typical CDCs in systems with different pore size distribution. If the capillary number is increased beyond a particular value, named critical capillary number, then the viscous forces will overcome the capillary forces which are responsible for holding the oil in the porous media. Consequently, residual oil saturation is decreased.

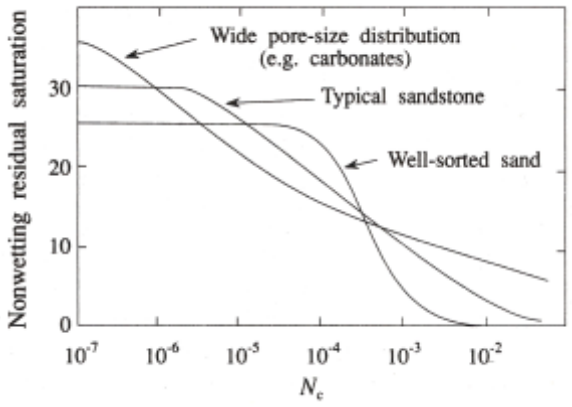

Figure 3.4 Capillary Desaturation Curve (Skjæveland and Kleppe, 1992).

The capillary number can be increased either by reducing the capillary forces or increasing the viscous forces. Under actual reservoir conditions, the viscous forces cannot be increased greatly because of the limitation on the injection pressure, which must not exceed the fracturing pressure of the formation. As a result, fluid velocities within the reservoir are generally limited to values of the order of 1 to 2 ft/day (Morrow, 1979).

The capillary forces, which are proportional to capillary pressure (P_c), are responsible for holding fluids in porous media. As shown by Equation 3.4, it can be reduced by decreasing IFT. Generally, IFT between water and oil can be in the range of 20 to 30 dynes/cm. By using an appropriate surfactant system, this IFT can be reduced to 10^{-3} or 10^{-4} dynes/cm.

$$P_c = \frac{2 \times IFT \times \cos\theta}{r} \tag{3.4}$$

Where IFT = interfacial tension between oil and water, θ = contact angle, and r = size of capillary.

Figure 3.5, taken from Gilliland and Conley (1976), illustrates the typical process of a surfactant flooding. Surfactant flooding is normally applied after waterflooding. Surfactant solution is relatively expensive, so a limited volume (slug size) is usually used. The surfactant slug therefore has to be displaced by water, usually containing polymer to reduce its mobility. An oil bank will start to flow and mobilize any residual oil in front. Behind the oil bank, the surfactant prevents the mobilized oil from being retrapped. If the surfactant concentration is large enough, oil and water will be completely miscible hence no residual oil will be left in the swept region. This is not a viable process, because it requires a large amount of surfactant. If the surfactant is injected at low concentration, there may be up to three phase mixture (oil, microemulsion, and water). In such condition, small amount of residual oil will still be trapped in the swept region.

In some instances, polymer and alkaline can also be added into the surfactant slug to improve the quality of the slug. Polymer is added to increase the slug viscosity, thus improving volumetric displacement efficiency. Addition of alkaline into the surfactant slug could reduce the required amount of the surfactant as the alkaline reacts with natural acids present in certain crude oils to form surfactants within the reservoir. The surfactants formed in the reservoir work in the same way as an injected surfactant.

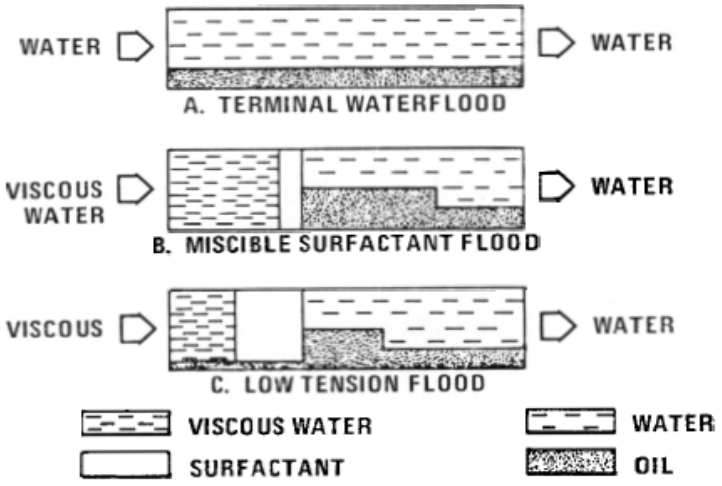

Figure 3.5 Surfactant flooding process (Gilliland and Conley, 1976).

3.4 Important Factors in Surfactant Flooding

Surfactant solution, or usually called microemulsion, behavior is complex and dependent on a number of parameters. Several parameters which are necessary to be considered in designing and executing surfactant flooding project are presented in this section.

3.4.1 Salinity

Figure 3.6, taken from Healy et al. (1976), shows the effect of brine salinity on surfactant solution (microemulsion) phase behavior. At low brine salinity, the surfactant is solubilized in the water phase, creating a lower phase microemulsion. At high salinity, the surfactant is driven out of the brine and solubilized in the oil phase. In this case, the microemulsion is an upper phase microemulsion. At intermediate salinity, the system separates into three phases. The microemulsion resides as a middle phase which is saturated with both oil and water. The salinity at which the middle phase microemulsion contains an equal volume of oil and water is defined as the optimal salinity for phase behavior (Healy et al., 1976).

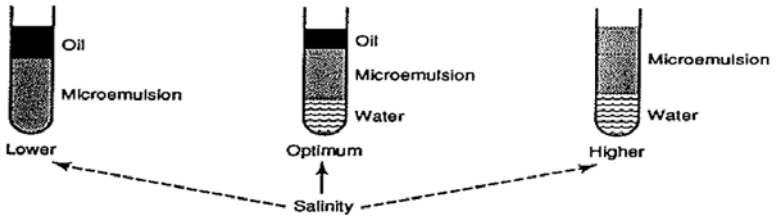

Figure 3.6 Effect of salinity on microemulsion phase behavior (Healy et al., 1976).

Figure 3.7, taken from Healy and Reed (1977), is a typical plot of IFT between equilibrium phases and final oil saturation (S_{of}) as a function of salinity. σ_{mo} and σ_{mw} represent microemulsion-oil IFT and microemulsion-water IFT, respectively. The value of salinity at which $\sigma_{mo} = \sigma_{mw}$ is called the optimal salinity for IFT (Healy et al., 1976). The authors reported that the optimal salinity for IFT is usually very close to the optimal salinity for phase behavior. The maximum oil recovery (minimum S_{of}) occurs at a salinity at or very near optimal salinity. These results show that a surfactant flooding is most efficient when the IFT between phases is low at both the leading and trailing edges of a surfactant slug. If the microemulsion-oil IFT is too large, oil will not be displaced efficiently by the slug. On the other hand, if the microemulsion-water IFT is too large, a relatively large residual saturation of surfactant will be trapped at the trailing edge of the slug and the slug will be degraded as it is transported through the rock.

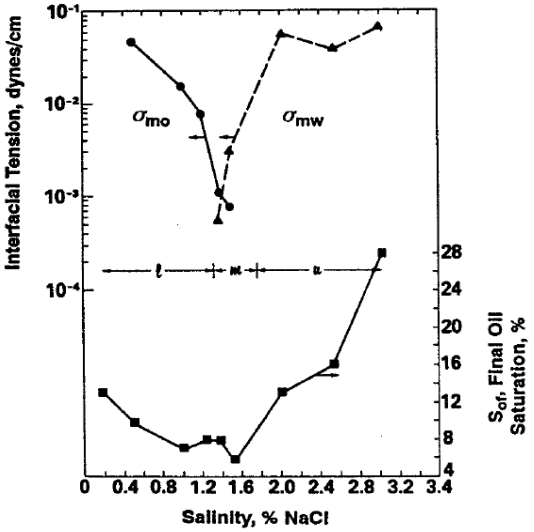

Figure 3.7 IFT and final oil recovery as a function of salinity (Healy and Reed, 1977).

3.4.2 Relative Permeability

Bardon and Longeron (1980) investigated the influence of IFT on gas-liquid relative permeabilities and the results are presented in **Figure 3.8**. The relative permeability curves become less curved as the gas-oil IFT is decreased. In addition, at any given saturation the relative permeability is generally higher when the IFT is lower. At very low IFT, the relative permeability curves are represented by two symmetrical diagonal lines, intersecting at 50% saturation. According to the authors, it occurs because viscous forces in the absence of capillary forces would cause uniform distribution of each phase in every capillary, in a

proportion corresponding to its saturation. When the capillary forces are present, the viscous forces would distribute the phases in the largest capillaries where the velocity is highest, while in the smaller capillaries the distribution of the different phases is still determined by the capillary forces.

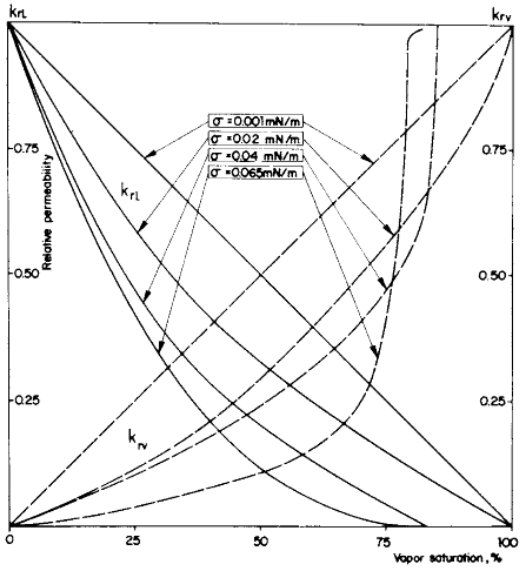

Figure 3.8 Gas-oil relative permeability curves for various IFT values (Bardon and Longeron, 1978).

Similar results were presented by Batycky and McCaffery (1978). They conducted a series of displacement processes for three water-oil IFT values which are nominally 50, 0.2, and 0.02 dynes/cm. They found that IFT reduction causes the relative permeability curves to become less curved. A reduction in IFT also causes a reduction and the eventual removal of hysteresis in the measured relative permeability curves. At IFT of 0.02 dynes/cm, the hysteresis completely disappears, however the relative permeability curves are still slightly curved.

3.4.3 Wettability

Garnes et al. (1990) measured capillary desaturation curves measured on different North Sea sandstone formations. The authors found that the North Sea Brent cores have lower critical capillary number compared to Berea cores. Therefore, smaller change in capillary number was required to mobilize the residual oil. They described that the more mixed wet behaviour and the higher permeability of the North Sea Brent cores may account for this lower critical capillary number.

Han Dong et al. (2006) conducted an experimental study to investigate waterflooding, Alkaline/Surfactant/Polymer (ASP) flooding, and polymer flooding performance in different wettability preferences. They found that displacement efficiency of waterflooding and ASP flooding is greatly affected by the wettability of the core, but displacement efficiency of polymer flooding is not sensitive to wettability. The oil recovery of waterflooding is optimum at close to neutral wettability while water wet and oil wet conditions are favourable to obtain high enhanced oil recovery for ASP flooding. Unfortunately, mixed wettability was not included in their experiment.

3.4.4 Surfactant Loss

Green and Willhite (1998) reported that surfactant loss from an injected surfactant slug can occur by at least three processes; precipitation, adsorption onto the porous medium, and phase partitioning into a static or slow moving phase. These mechanisms result in retention of surfactant in porous medium and deterioration of the surfactant composition, leading to poor displacement efficiency.

The adsorption is strongly affected by the surfactant concentration. **Figure 3.9**, taken from Skjæveland and Kleppe (1992), shows the typical adsorption isotherm for the adsorption of a negatively charged surfactant onto positively charged adsorbent. As the surfactant concentration increases, the adsorption increases until CMC is reached. Surfactant addition above CMC will create micelles, but the amount of monomers is constant. According to the authors, the micelles do not adsorb onto the solid, therefore surfactant adsorption is constant above CMC.

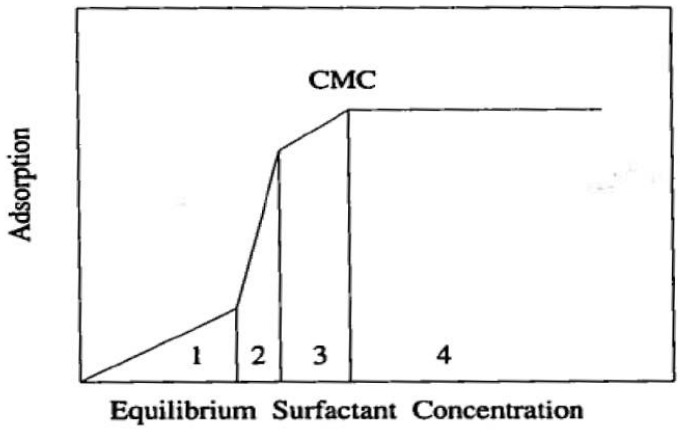

Figure 3.9 Surfactant adsorption as a function of surfactant concentration (Skjæveland and Kleppe, 1992).

3.4.5 Gravity Segregation

Morrow (1979) presented an analysis to study the interplay of capillary, viscous, and buoyancy forces in the mobilization of residual oil. The author found that the value of water-oil IFT below which the oil droplet is mobilized, calculated by equating the hydrostatic pressure difference with the capillary pressure difference, is equal to 10^{-3} dynes/cm. That is the same order of magnitude as the IFT lowering needed to mobilize oil by viscous forces when the flooding rates were restricted to field rates of about 1 ft/day. These results demonstrate that the trapped oil mobilization could occur because of viscous or buoyancy forces or some combination of both.

Morrow and Songkran (1982) investigate the correlation between Bond number (N_B) and oil recovery. Bond number is a dimensionless ratio between buoyancy and capillary forces, in the form of equation it can be expressed as shown by **Equation 3.5**.

$$N_B = \frac{\Delta\rho g R^2}{IFT} \tag{3.5}$$

Where $\Delta\rho$ = oil-water density difference, IFT = oil-water interfacial tension, g = gravitational constant, R = characteristic length. **Figure 3.10** shows plots of residual oil saturation as a function of inverse Bond number at various capillary numbers. For the type of system under their study, it was estimated that zero residual oil saturation will occur if the inverse Bond number is less than about 3. When the inverse Bond number is greater than about 200, gravity forces have no effect on the residual oil saturation, and the residual oil saturation depends only on capillary number. These results demonstrate that the capillary pressure can also be overcome by buoyancy forces.

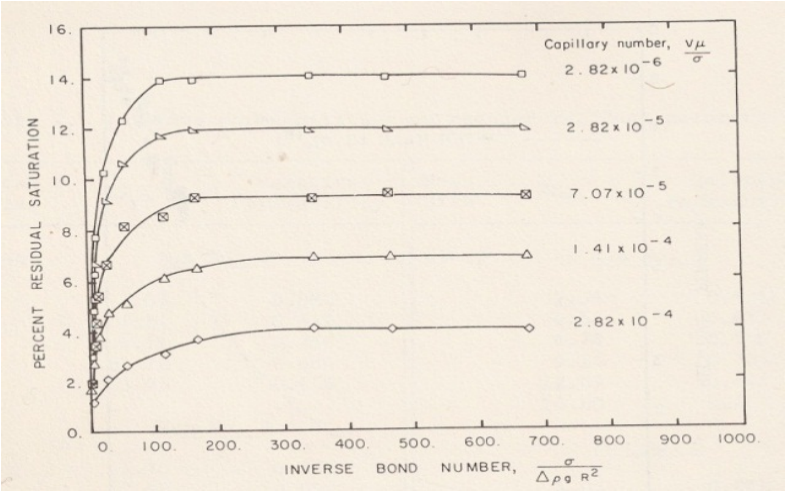

Figure 3.10 Residual oil saturation as a function of inverse Bond number (Morrow and Songkran, 1982).

Hornof and Morrow (1987) observed front instabilities in displacement process at low water-oil IFT, even the mobility ratio was at a favorable value. According to the authors, the instabilities are caused by gravity segregation, which occurs if capillary and viscous forces are insufficient to overcome the effect of buoyancy forces. These experiments reveal that the degree of gravity segregation tends to increase with a decrease in IFT.

Schechter et al. (1991) investigated the effect of reduced IFT on gravity segregation in an imbibition process. The authors found that a transition from capillary to gravity driven flow occurred as the IFT was reduced. For low IFT and high permeability cores, buoyancy forces might play a significant role in displacement mechanism. The authors also found that as the inverse Bond number was decreased, an oil droplet that would have been trapped in the capillary dominated flow could continue to flow if the gravitational forces became more dominant.

4 METHODOLOGY AND MODEL SETUP

Nowadays, reservoir simulation is a very common practice in oil and service companies which is used by most reservoir engineers. It is a very useful tool for estimating the future behaviour of petroleum fields. In some cases, it can also be used for identifying particular phenomena in a specific task.

All investigations in this study were performed by means of numerical simulation experiments. Eclipse black oil model with surfactant option was used for simulating the displacement process. In addition, Flow2D was also used for upscaling the relative permeability curves. In the following sections, an overview about Eclipse and the methodology carried out in this study are discussed.

4.1 Eclipse Overview

Eclipse is a reservoir simulator owned by SIS, a division of Schlumberger. It consists of two separate simulators; Eclipse 100 for black oil modelling, and Eclipse 300 for compositional modelling (Eclipse Technical Description, 2009). All simulations in this study were conducted using the Eclipse 100. It is fully implicit, three phases, three dimensional, and generally used for black oil modelling. The black oil model treats hydrocarbons as if they have 2 components (oil and gas). Black oil model can be used whenever the hydrocarbon compositions and properties do not vary significantly with pressure.

Eclipse 100 has the options to simulate several chemical species (polymer, surfactant, alkaline, solvent, and foam). The surfactant option is the one that being employed in this study. The important features of surfactant flooding can be modelled with this option. These important features are discussed later in **Section 4.1.1**.

In this work, the input data for Eclipse simulation were prepared in free format using TextPad. This text editor offers interesting features which improve user's productivity when dealing with a lot of data files. An Eclipse data input file is divided into the following sections;

1. RUNSPEC

   This is the first section of an Eclipse data input file. It contains the run title, start date, units, various problem dimensions (number blocks, wells, tables, etc.), flags for phases present (oil, water, gas) and option switches (surfactant, polymer, etc.).

2. GRID

   This section defines the basic geometry of the simulation grid and various rock properties (porosity, absolute permeability).

3. PROPS

   This section contains pressure and saturation dependent properties of the reservoir fluids and rock. In surfactant model, properties of the surfactant must be provided in this section as well. The saturation dependent properties include relative permeability and capillary pressure data. The pressure dependent properties include formation volume factor, density, and viscosity.

4. REGIONS

   This section divides the computational grid into regions. In surfactant model, the computational grid is divided into miscible and immiscible conditions. Different sets of saturation functions corresponding to miscible and immiscible conditions are assigned to the grid.

5. SOLUTION

   This section defines the initial state (pressure, water-oil contact) of every grid block in the reservoir.

6. SUMMARY

   This section specifies a number of variables that are to be written to Summary files after each time step of the simulation.

7. SCHEDULE

   This section specifies the operations to be simulated (production and injection controls, and constraints) and the times at which output reports are required. Simulator tuning parameters may also be specified in this section.

4.1.1 Surfactant Model in Eclipse

The surfactant option can be activated by using SURFACT keyword under RUNSPEC section. The surfactant is assumed to exist only in the water phase, so the amount of the surfactant injected into the reservoir is specified as a concentration at a water injector by using WSURFACT keyword under SCHEDULE section. The surfactant concentration will

determine the oil-water IFT based on a table provided by SURFST keyword under PROPS section. The table supplies IFT as a function of surfactant concentration in the injected water.

The surfactant model does not provide detailed chemistry of a surfactant process, but it has the capability to model the important features of a surfactant flooding on a full field basis (Eclipse Technical Description, 2009). These important features include:

1. Reduction of capillary pressure.

   Eclipse uses the value of IFT for calculating the capillary pressure. The capillary pressure is given by the following equation.

$$P_{cow} = P_{cow}(S_w)\frac{IFT(C_{surf})}{IFT(C_{surf} = 0)} \tag{4.1}$$

   Where P_{cow} = oil-water capillary pressure, $IFT(C_{surf})$ and $IFT(C_{surf} = 0)$ = oil-water interfacial tension at the present and zero surfactant concentration, respectively. J function is a dimensionless group that allows the capillary pressure to be correlated with the rock properties. In many cases, all of the capillary pressure data from a formation will be reduced to a single curve when the J function is plotted against the saturation. If J function data are used, then an additional keyword (JFUNC) will be required under GRID section to convert J function data into capillary pressure values based on **Equation 4.2**.

$$P_c = J(S_w) \times IFT \times \left(\frac{\emptyset}{k}\right)^{0.5} \times U_{const} \tag{4.2}$$

   Where P_c = capillary pressure, $J(S_w)$ = dimensionless capillary pressure, U_{const} = unit conversion constant, $\emptyset$ and k = porosity and permeability, respectively.

2. Alteration of relative permeability curves from immiscible to miscible condition.

   The capillary number is also calculated based on IFT. As the capillary number increases, there will be a transition from immiscible to miscible condition. The user has to provide a surfactant capillary desaturation function which describes the

transition from immiscible to miscible condition as a function of the capillary number. It is done by implementing SURFCAPD keyword under PROPS section.

Relative permeability curves are modified based on the capillary number. The modification is essentially a transition from immiscible relative permeability curves (at low capillary number) to miscible relative permeability curves (at high capillary number). Relative permeability curves for both miscible and immiscible condition must be provided in PROPS section.

Figure 4.1 illustrates the calculation of the relative permeability curves for oil phase. The end points of the curve are interpolated and both the immiscible and the miscible curves are scaled to honour these points. The relative permeability values are looked up on both curves, and the final relative permeability is taken as an interpolation between these two values. The relative permeability for the water phase is calculated in the same way as the oil case.

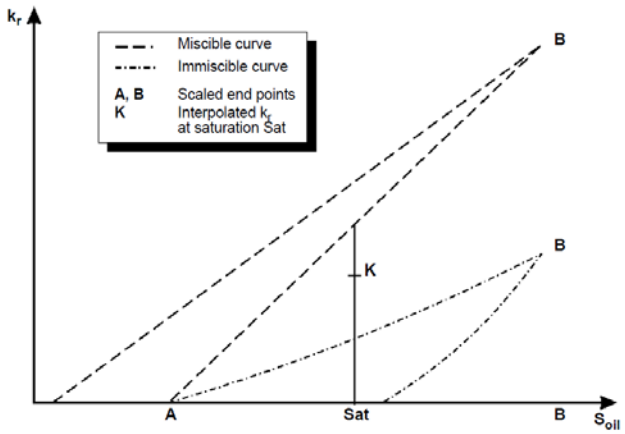

Figure 4.1 Calculation of the relative permeability (Eclipse Technical Description, 2009).

3. Alteration of the injected water viscosity due to surfactant addition.

   The surfactant also changes the viscosity of the injected water. The surfactant viscosity must be provided as a function of surfactant concentration using SURFVISC keyword under PROPS section. Eclipse uses this input for calculating the water-surfactant solution viscosity based on the following equation.

$$\mu_{ws}(C_{surf}, P) = \mu_w(P)\frac{\mu_s(C_{surf})}{\mu_w(P_{ref})} \quad (4.3)$$

Where μ_{ws} = water-surfactant solution viscosity, μ_s = surfactant viscosity, and μ_w = water viscosity.

4. Alteration of wettability.

   This feature enables the modelling of wettability alteration of the rock due to the accumulation of the surfactant. It can be activated by using SURFACTW keyword.

5. Surfactant adsorption onto the surface of reservoir rock.

   In addition to the keywords mentioned above, the other optional keywords for surfactant modelling in Eclipse include SURFADS and SURFROCK. Both of the keywords are intended for describing the tendency of the surfactant to be adsorbed by the reservoir rock.

4.2 Methodology

As described in the previous section, Eclipse surfactant model has the capability to model the main features of a surfactant flooding process. These main features include:

1. Reduction in capillary pressure.
2. Alteration of relative permeability curves from immiscible to miscible condition.
3. Alteration of the injected water viscosity due to surfactant addition.
4. Alteration of rock wettability.
5. Surfactant adsorption onto the surface of reservoir rock.

This study was intended to investigate the effect of capillary pressure on gravity segregation. To achieve this purpose, Eclipse black oil simulator was used and surfactant option was activated to introduce the reduction in capillary pressure (by reducing IFT). In order to isolate the mechanism of capillary pressure reduction from the other mechanisms, the Eclipse surfactant model's feature no.2 through no.5 need to be turned off.

The feature no.2 was turned off by using the same set of saturation functions both for miscible and immiscible condition. The feature no.3 was excluded by specifying the same viscosity both for water and water-surfactant solution. The features no.4 and 5 were neglected by excluding any keywords related to these features.

Additionally, the surfactant solution was injected continuously. In such situation, the reduction in IFT will follow the water front and be constant behind the water front. This will allow us to conveniently assess the effect of any single parameter at a specific IFT without worrying about the interference from IFT alteration during the displacement process.

4.3 Base Case Design

In this section, all input parameters used in base case model are presented. The input parameters include model geometry, rock and fluids properties, saturation functions, wells and simulation controls. The complete Eclipse input data for the base case can be found in **Appendix A**.

4.3.1 Model Geometry and Rock Properties

A synthetic cross sectional two-dimensional (2D) model with one injection and one production well was created to investigate the possible effects of gravity segregation on oil recovery. A schematic representation of the model is shown in **Figure 4.2**.

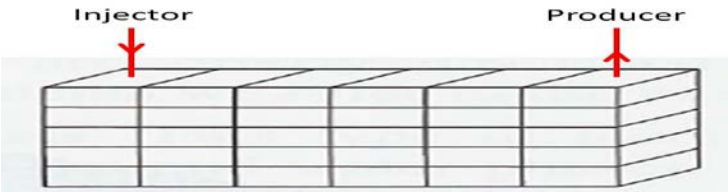

Figure 4.2 Schematic representation of the synthetic model and the wells (not to scale).

Table 4.1 presents the geometry and rock properties data used for building the base case model. The model consists of 20 layers with uniform porosity of 25%, uniform horizontal and vertical permeability of 1000 and 250 md, respectively. The rock has a very low compressibility, such that the rock volume will not be affected by pressure changes. The length of the model is much larger than the thickness which is intended to give sufficient time

for gravity forces to act on the system. This thin model may represent a single layer of a reservoir.

Table 4.1 Geometry and rock properties data for base case.

Property	Value
Length	500 m
Width	5 m
Height	2 m
Grid Dimension	100x1x20
Porosity	0.25
Horizontal permeability	1000 md
Vertical permeability	250 md
Rock Compressibility	1E-9 bar^{-1}

4.3.2 Fluid Properties

Two phases (oil and water) were involved in the simulation. **Table 4.2** summarizes the properties of the fluids. Both the oil and water phase are assumed to be incompressible, such that their Formation Volume Factors (FVF) were set at a value of 1 rm^3/sm^3 at all pressures. Water and water-surfactant solution viscosity were set at the same value of 0.3 cp.

Table 4.2 Fluid properties.

Property	Value
B_w	1 rm^3/sm^3 at all pressure
B_o	1 rm^3/sm^3 at all pressure
ρ_o	600 kg/m^3 at STP
ρ_w	1000 kg/m^3 at STP
μ_o	0.5 cp at all pressure
μ_w	0.3 cp at all pressure
μ_{ws}	0.3 cp at all SC

4.3.3 Surfactant Properties

Table 4.3 summarizes the IFT as a function of surfactant concentration. Plot of the data is presented in **Figure 4.3**. As can be seen, surfactant concentration of 6 kg/m^3 is considered as the CMC of the surfactant system, in which further surfactant addition above this value will not change the IFT.

Table 4.3 IFT as a function of surfactant concentration.

Surf Conc, kg/m3	IFT, dynes/cm
0	25
0.5	1
1.5	0.1
3	0.01
6	0.001
10	0.001

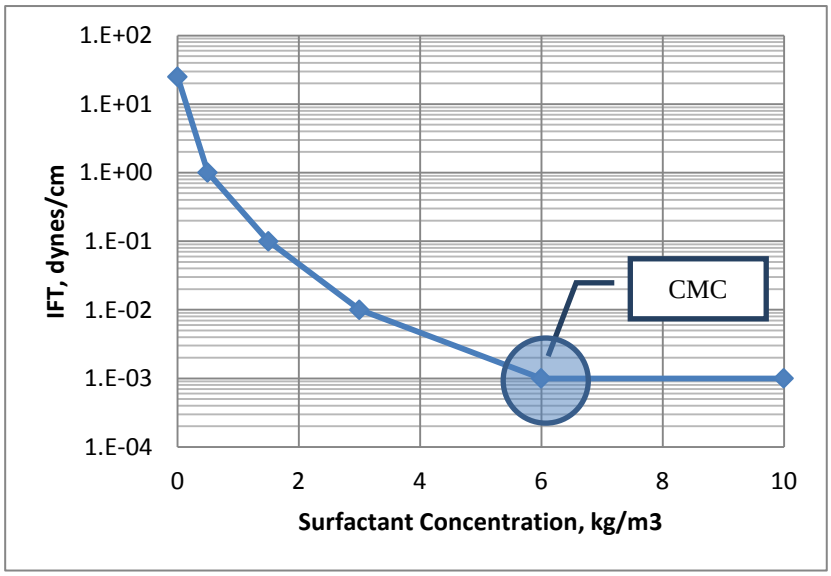

Figure 4.3 IFT as a function of surfactant concentration.

Table 4.4 gives the surfactant capillary desaturation data. In Eclipse, the water-oil miscibility is expressed by a number between 0 and 1. A value of 0 implies immiscible condition and a value of 1 represents miscible condition. It is worth to emphasize that the surfactant capillary desaturation data will not affect the results in this study since the same saturation functions apply for both immiscible and miscible condition.

Table 4.4 Surfactant capillary desaturation data.

Log Nc	Miscibility
-9.00	0.00
-4.50	0.00
-2.00	1.00
10.00	1.00

4.3.4 Saturation Functions

The relative permeability and capillary pressure data were taken from a mixed wet core from a North Sea reservoir. **Figure 4.4** shows the plot of relative permeability as a function of water saturation in linear and logarithmic scale whereas the plot of the imbibition dimensionless capillary pressure (J function) as a function of water saturation is presented in **Figure 4.5**. These data were used for both miscible and immiscible conditions.

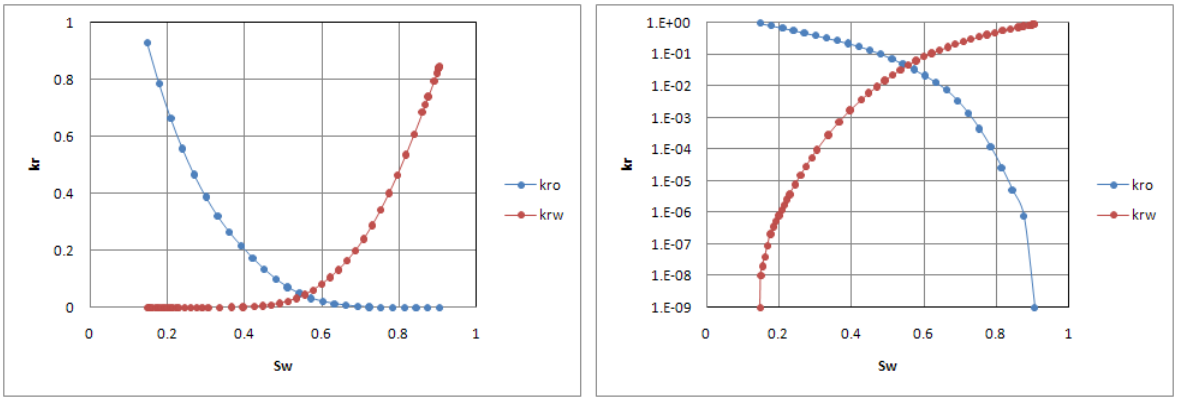

Figure 4.4 Mixed wet relative permeability in linear (left) and logarithmic scale (right).

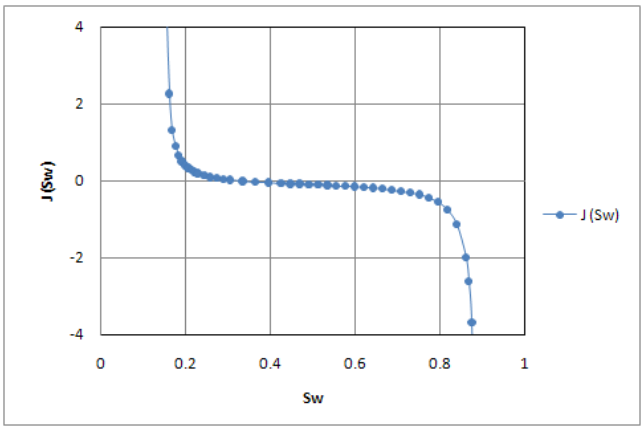

Figure 4.5 Mixed wet dimensionless imbibition capillary number.

As can be seen in **Figure 4.4**, the relative permeability curves for both of the oil and water phase have high curvature, low residual saturation, and long tail at low saturation. Additionally, the end point water and oil relative permeability are comparable (0.85% and 0.93% of absolute permeability, respectively). **Figure 4.5** shows that the capillary pressure becomes negative as the water phase saturation increases. Those are the typical characteristics of a mixed wet system.

4.3.5 Wells and Simulation Controls

Boundary conditions were set using two wells, placed in the first and the last block (see **Figure 4.2**) with well connection factors corresponding to open end faces. Open end faces were implemented to exclude the additional pressure drop due to the wells, so the simulation would resemble displacement process in a particular part of a reservoir. It was done by calculating the Well Connection Factor (WCF) with the following equation and using it as an input parameter under COMPDAT keyword.

$$\mathrm{WCF} = \frac{\mathrm{k_h A}}{\left(\frac{\Delta x}{2}\right)} \tag{4.4}$$

Where $\mathrm{k_h}$ = horizontal permeability, A = cross sectional area, and Δx = grid block size in x direction. Both of the wells were perforated in all layers. The production well was controlled by minimum bottomhole pressure of 200 bars, while the injection well was controlled by the injection velocity of 0.5 m/day. However, Eclipse does not provide injection velocity as a well controlling parameter. Therefore, the injection fluid velocities were converted into injection rates, and then included in the Eclipse input data by using RESV keyword.

5 RESULTS AND DISCUSSION

5.1 Simulation Model Validation

As a starting point, the simulation model is validated by evaluating the effect of IFT on oil recovery in a mixed wet one-dimensional (1D) horizontal model. Two IFT values were used (25 and 1 dynes/cm) and both of the cases were run at the same injection velocity of 0.5 m/day. The production profiles for both of the cases are presented in **Figure 5.1**. There are at least two observations that can be made from these results. First, most of the oil production occurs before water breakthrough. However, considerable amount of oil production is also observed after the water breakthrough. The recovery factor at 5 PV injected is about 73% and keeps increasing if the water injection continues. The continuously increasing oil production after water breakthrough occurs because the oil wet surfaces in the larger pores of the mixed wet system help maintaining the continuity of oil phase at low oil saturation. These results possess a similar trend as the characteristic of mixed wet reservoir as reported by Salathiel (1973).

The second observation is that both of the cases give the same production profiles. It is expected since the same saturation functions are used for both immiscible condition (at high IFT) and miscible condition (at low IFT). Additionally, it is expected that there was no vertical gravity segregation acting in the one-dimensional system because the fluids were allowed to move in horizontal direction only. These results suggest that gravity segregation is the only mechanism that will be affected by changing IFT in this simulation model. Isolating gravity segregation from other mechanisms is very important, since this study focuses on investigating the mechanism of gravity segregation.

5.2 Effect of Gravity Segregation on Oil Recovery

Two runs were created using the two-dimensional base case model with high (25 dynes/cm) and low (1 dynes/cm) IFT. Both of the cases were run at the same velocity of 0.5 m/day. **Figure 5.2** shows the production profiles from both of the cases, along with the result from the one-dimensional model. It can be seen that the final oil recoveries from both of the two-dimensional models are higher than that given by the one-dimensional model. The highest oil recovery is given by the two-dimensional model with low IFT, 78% of IOIP, while the two-dimensional model with high IFT has produced almost 73%, and the one-dimensional model has recovered 69% of IOIP after 5 PV injected.

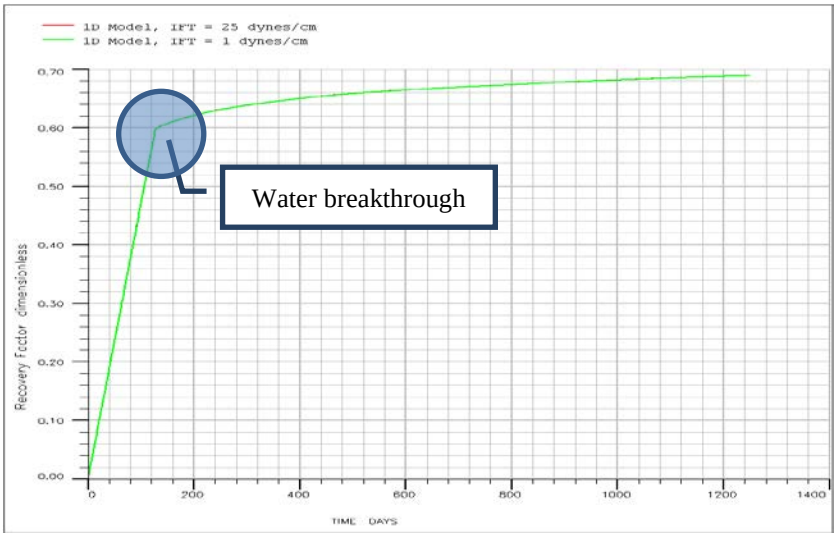

Figure 5.1 Production profiles from 1D model with IFT of 1 and 25 dynes/cm. The curve for IFT of 25 dynes/cm is not seen due to overlap with the other curve.

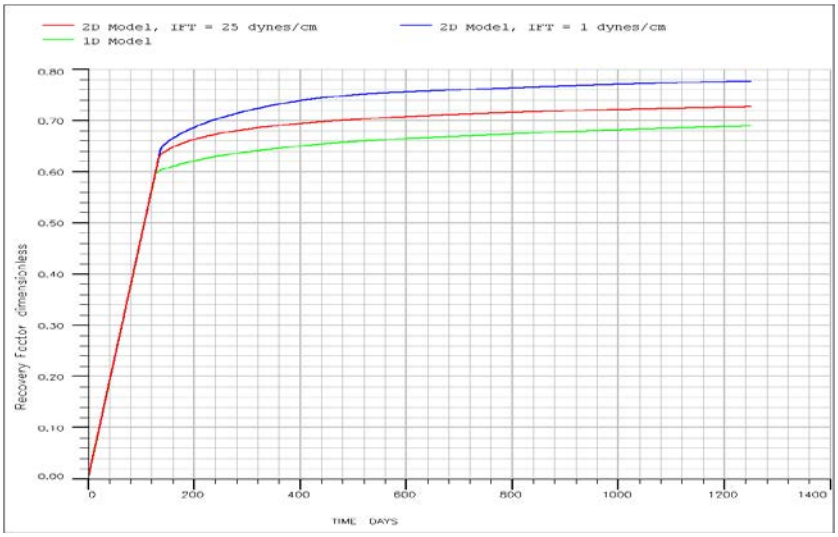

Figure 5.2 Production profiles from 1D and 2D model with IFT of 25 and 1 dyne/cm.

The oil recovery mechanisms in those three cases would be better understood by investigating their oil saturation distributions. **Figure 5.3** visualizes the oil saturation distribution after 5 PV injections for all of the three cases. In the case of one-dimensional model, no gravity segregation is observed because the fluids moved in horizontal direction only (see **Figure 5.3a**). The oil saturation is lower at the inlet (the injection well) and increases toward the outlet (the production well). The oil phase was displaced solely by horizontal viscous forces toward the production well.

In both of the two-dimensional models, vertical gravity segregations are observed. Gravity forces cause the less dense phase (oil) to move upward and the denser phase (water) to move downward. This condition results in an upward increasing trend in oil saturation. More even distribution of oil saturation is observed in the model with high IFT (see **Figure 5.3b**) when compared with the model with low IFT (**Figure 5.3c**). In the model with low IFT, most of the oil phase has travelled to the top of the model creating a very thin layer with high oil saturation. These results clearly demonstrate that gravity segregation acting behind the displacement front may increase the oil recovery by accumulating the oil phase at the top of the model, thus improving the effective horizontal oil mobility. Capillary forces will act against this segregation. A reduction in IFT will decrease the capillary forces, thus increasing the magnitude of gravity segregation. Further investigations on the effect of IFT on gravity segregation are discussed later in **Section 5.4**.

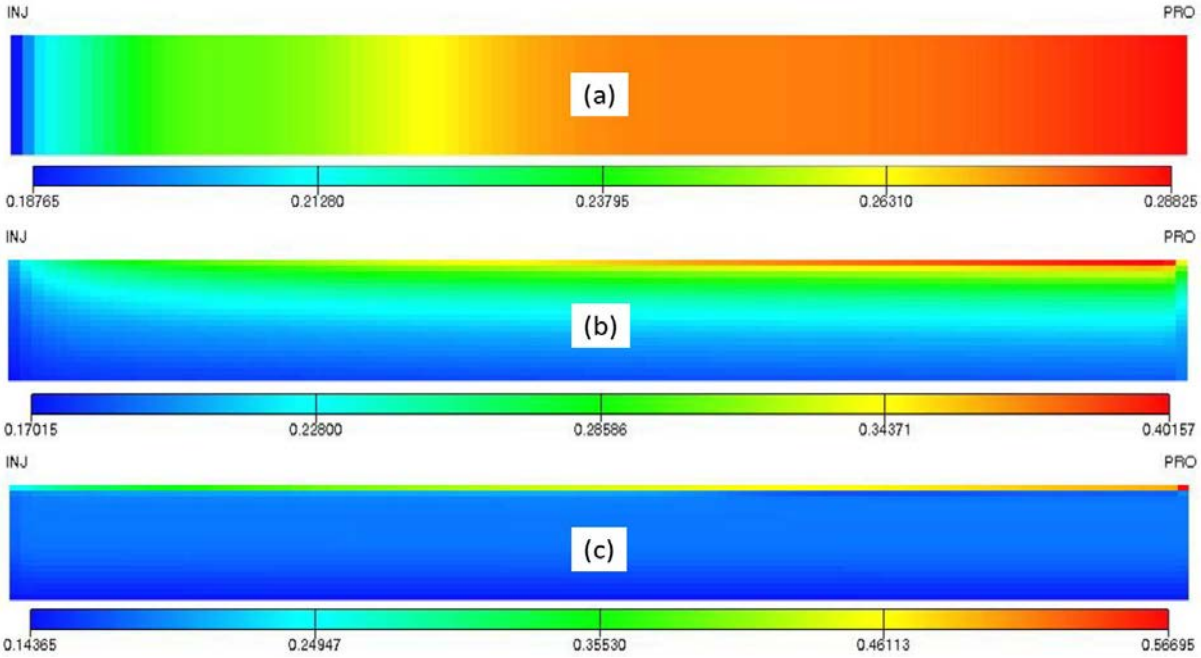

Figure 5.3 Oil saturation distributions in (a) 1D model, and 2D models with IFT of (b) 25 dynes/cm and (c) 1 dynes/cm.

5.3 Effect of Injection Velocity on Gravity Segregation

A series of simulations was made using the base case model with five different velocities ranging from 0.05 to 500 m/day and IFT of 25 dynes/cm. **Table 5.1** summarizes the key parameters involved in this simulation. The oil recoveries at 5 PV injected as functions of velocities are presented in **Figure 5.4**. As shown by the lower plateau, at high velocity the oil recovery is independent on the velocity. This lower plateau acts as a lower limit of the oil recovery in the system. As the velocity is decreased, the oil recovery increases until an upper plateau is reached. It should be noted that the curve has not exactly reached an upper plateau, but it is expected to reach an upper plateau at further reduction in velocity. The upper plateau acts as an upper limit of the oil recovery. The velocity where the curve starts to deviate from the lower plateau is further considered as the critical velocity.

These results demonstrate that gravity segregation is a slow process. Low injection velocity must be applied to allow sufficient time for the gravity forces to act in the system. There is a critical velocity above which the gravity segregation will not be observed. A reduction in velocity below the critical value will improve the degree of gravity segregation until gravity and capillary forces reach an equilibrium condition.

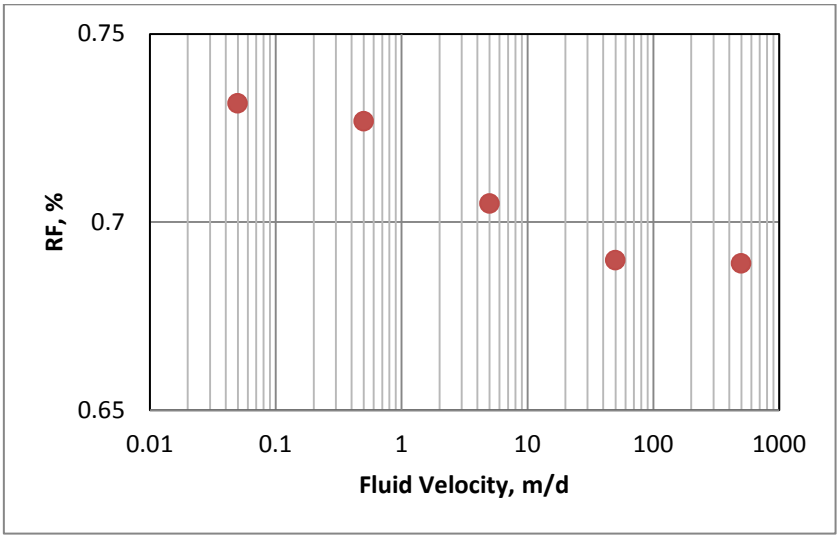

Figure 5.4 Oil recovery factor as a function of velocity from the base case simulation.

Table 5.1 Key parameters in the base case model.

Key Parameters	Value
IFT	25 dynes/cm
Vertical permeability	250 md
Horizontal permeability	1000 md
Oil density	600 kg/m3
Model thickness	2 m

As stated previously, the curve is expected to reach an upper limit at further decrease in velocity. However, oil recoveries at injection velocities below 0.05 m/day are not provided since some numerical difficulties were encountered when running the simulations at extremely low injection velocities. Vertical Equilibrium (VE) steady state upscaling method was then implemented to estimate the upper limit. In this study, the upscaling was performed by using the IRIS in-house Flow2D software.

Flow2D was specifically used to upscale the relative permeability curves from the original saturation distribution to a saturation distribution that satisfies vertical equilibrium between gravity and capillary forces. The upscaled VE properties are normally considered as pseudo-properties, because they are valid only for a system with a given thickness, density difference, and capillary pressure functions. The upscaled relative permeability curves along with the original ones are shown in **Figure 5.5**. It is clearly seen that the upscaled curves are less curved than the original ones. At any given saturation, the upscaled relative permeability is generally higher than the original one. The complete input data set for Flow2D upscaling in the base case model can be found in **Appendix B**.

Figure 5.6 shows the same results as presented in **Figure 5.4**, together with recovery predicted by one-dimensional simulations using the original and upscaled VE relative permeabilities. At low velocities, the oil recovery approaches the level predicted by the VE properties. It shows that VE upscaling is good approach to predict the upper limit. At high velocities, the lower plateau coincides with the level predicted by the one-dimensional simulation using the original relative permeability. It confirms that gravity segregation will not occur when the velocity is above the critical value.

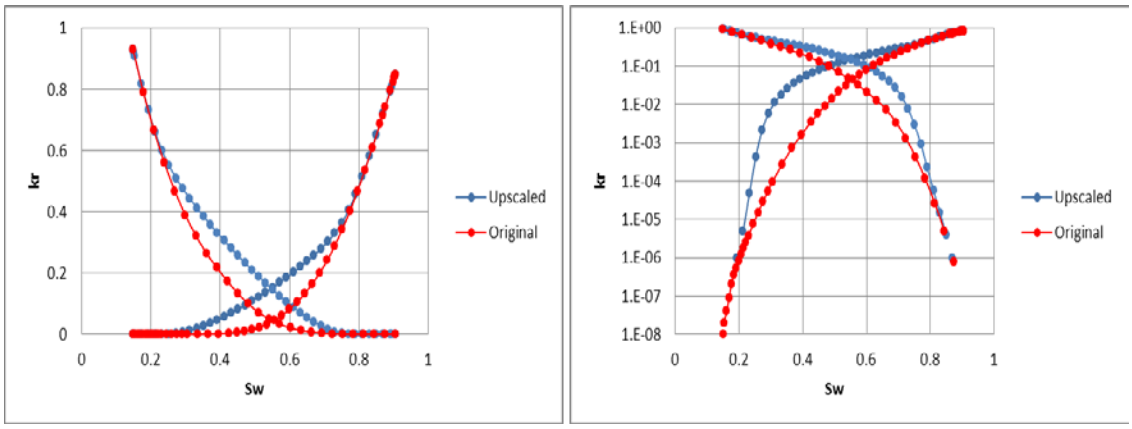

Figure 5.5 Upscaled VE curves for the base case model (IFT 25 dynes/cm) in linear and log scale.

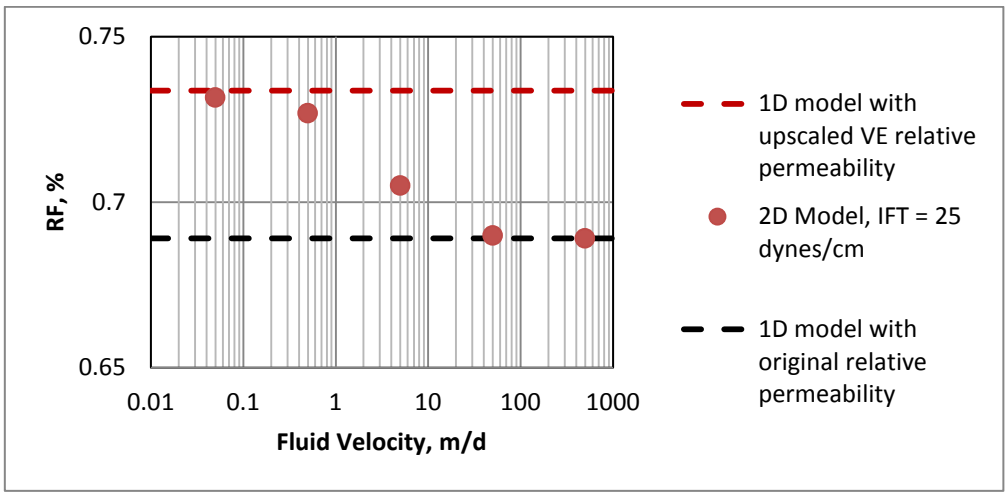

Figure 5.6 Oil recovery factor and the predicted upper and lower limit.

5.4 Effect of IFT on Gravity Segregation

In the previous section, a series of simulations was created using the base case model with high IFT (25 dynes/cm). Here, an additional series was made using the same model with low IFT (1 dynes/cm). The effects of IFT on gravity segregation were determined by comparing the level of the upper limit and the critical velocity between the high and low IFT model.

Figure 5.7 shows the results from both the low and high IFT, together with their predicted upper and lower limit. There are three main observations to make from these results. The first observation is that both of the systems have the same critical velocity of about 20 m/day, indicating that the critical velocity is independent on IFT. This value of critical velocity is a rough estimation; it might be lower if more points in the plot were used.

The second observation is that the effect of IFT reduction becomes more significant as the injection velocity is decreased. The third observation is that the upper limit significantly improves, from 73% to 85%, when the IFT is reduced from 25 to 1 dynes/cm. It indicates that capillary forces restrict the gravity segregation, thus reducing the capillary pressure (by reducing IFT) will increase the degree of gravity segregation.

The upper limit improvement was then calculated by using **Equation 5.1**. It was found that the upper limit increases by 16% when the IFT is reduced from 25 to 1 dynes/cm. Only a moderate reduction in IFT down to 1 dynes/cm (compared to standard surfactant flooding) was used in these simulations. These results show that there is a considerable potential increase in oil recovery given by gravity segregation mechanism. All the main observations from this base case simulation are summarized in **Table 5.2**.

$$\%\ \text{Upper Limit Improvement} = \left| \frac{(\text{Upper Limit})_{\text{High IFT}} - (\text{Upper Limit})_{\text{Low IFT}}}{(\text{Upper Limit})_{\text{High IFT}}} \right| \tag{5.1}$$

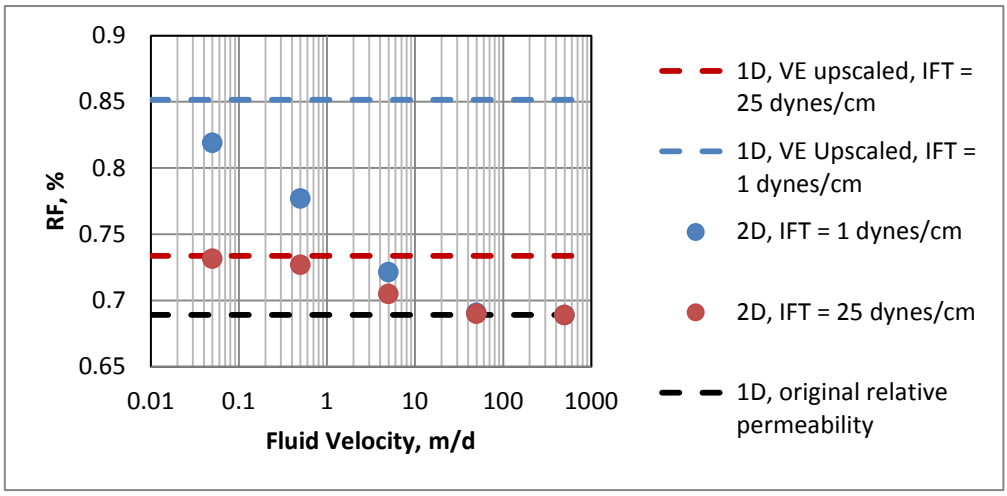

Figure 5.7 Oil recovery factor and the predicted upper and lower limit (k_v = 250 md, k_h = 1000 md, ρ_o = 600 kg/m^3, H = 2 m).

Table 5.2 Main observations from the base case simulation.

Observation	Result
Critical Velocity, m/day	~20
Upper Limit (IFT = 25 dynes/cm), %	73
Upper Limit (IFT = 1 dynes/cm), %	85
Upper Limit Improvement, %	16

The VE upscaled relative permeability curves for both the high and low IFT are presented in **Figure 5.8**. It can be seen that the low IFT's upscaled curves are represented by straight lines, whereas the high IFT's upscaled curves have somewhat strong curvature. This indicates that the capillary forces in the low IFT system are almost completely eliminated, as shown by the straight lines of the relative permeability curves. Therefore, the upper limit of the low IFT model is significantly higher than that given by the high IFT model.

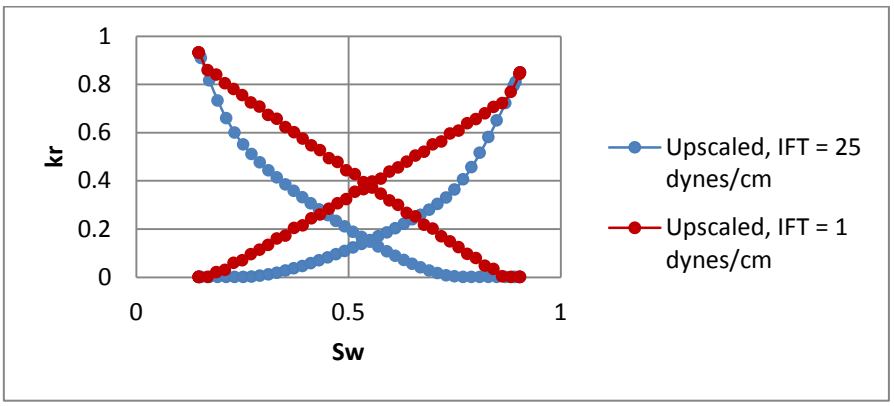

Figure 5.8 Upscaled VE relative permeability curves for the base case model with IFT of 25 and 1 dynes/cm.

5.5 Effect of IFT on Gravity Segregation in Various Conditions

The key parameters presented in **Table 5.1** are expected to affect the behaviour of gravity segregation. In this section, the effects of each of those parameters were investigated to study in what way they affect the segregation process. The investigations were performed by varying one parameter while the other parameters were kept unchanged. The simulation cases are summarized in **Table 5.3**. The highlighted parameter is the one being investigated in each case.

Table 5.3 Simulation cases.

Case Number	k_v, md	k_h, md	ρ_o, kg/m3	H, m
Base Case	250	1000	600	2
Case 1	1000	1000	600	2
Case 2	250	250	600	2
Case 3	250	1000	850	2
Case 4	250	1000	600	20

In each case, two series of simulations at various injection velocities were created. One series is for the model with high IFT (25 dynes/cm) and the other series is for the model with low IFT (1 dynes/cm). The corresponding upper and lower limits for the low and high IFT model were also created by one-dimensional simulations with original and upscaled VE relative permeability curves. The simulation results from each case were then compared with the results given by the base case model as shown in **Table 5.2**.

5.5.1 Case 1: Effect of Vertical Permeability

The simulation results from case 1 are presented in **Figure 5.9**. In this case, the vertical permeability is four times higher than that in the base case. The main observations from this case are summarized in **Table 5.4**. For comparison, the observations from the base case simulations are also presented in the same table.

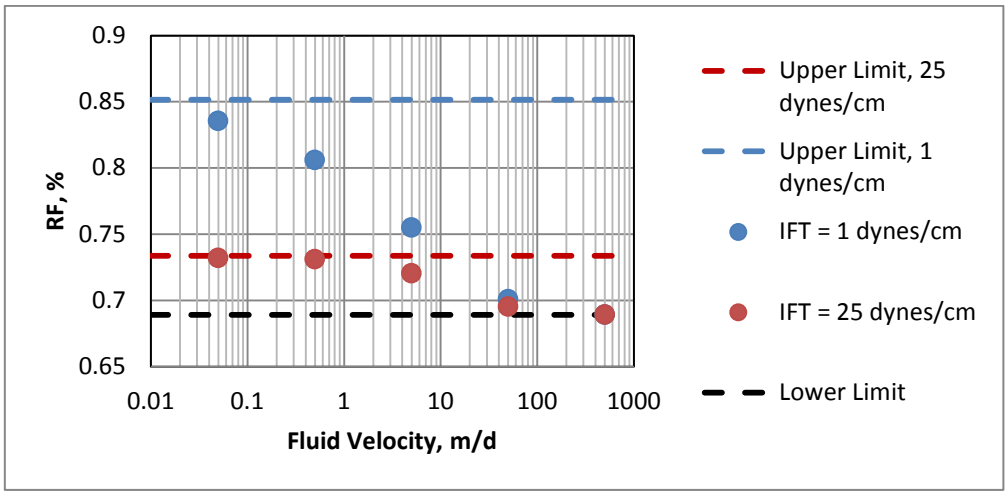

Figure 5.9 Simulation results from the case 1.

Table 5.4 Observations from the case 1 and the base case

Observations	Case 1, k_v = 1000 md	Base Case, k_v = 250 md
Critical Velocity, m/day	~80	~20
Upper Limit (IFT = 25 dynes/cm), %	73	73
Upper Limit (IFT = 1 dynes/cm), %	85	85
Upper Limit Improvement, %	16	16

The critical velocity for both the low and high IFT is estimated to be 80 m/day, which is four times higher than that given by the base case (20 m/day). These results demonstrate that

increasing the vertical permeability by a given factor will increase the critical velocity by the same factor.

Obviously, the lower limit is not affected by the vertical permeability. So are the upper limits for both the high and low IFT model. Flow2D calculates the J-scaling based on the following equation.

$$P_c = J \times IFT \times \sqrt{\frac{\emptyset}{k_x}} \tag{5.2}$$

Where Pc = capillary pressure, J = dimensionless capillary pressure, $\emptyset$ = porosity, and k_x = horizontal permeability in x direction. The equation shows that vertical permeability is not accounted for calculating the J-scaling of capillary pressure in the Flow2D software. Therefore, changing vertical permeability will not affect the upper and lower limit. However, at any given velocity between the upper and lower plateau, reducing IFT in the system with higher vertical permeability may give higher oil recovery improvement. For example, at velocity of 5 m/day, the case 1 gives almost 5% improvement of oil recovery by reducing the water-oil IFT from 25 to 1 dynes/cm, while the same reduction of IFT in the base case gives only about 2% improvement.

5.5.2 Case 2: Effect of Horizontal Permeability

The simulation results from case 2 are presented in **Figure 5.10**. In this case, the horizontal permeability is four times lower than that in the base case. The main observations from this case are summarized in **Table 5.5**. For comparison, the observations from the base case simulations are also presented in the same table.

Comparing the results from the case 2 and the base case, it can be observed that the horizontal permeability has no influence in the critical velocity. In both of the cases, gravity segregation occurs at the same velocity of about 20 m/day. It occurs simply because the horizontal permeability does not affect the vertical segregation rate.

The upper limit increases from 71 to 84 dynes/cm when the IFT is reduced from 25 to 1 dynes/cm. Both of those upper limits are slightly lower than those given by the base case

simulations. It occurs because the capillary pressure is inversely proportional to square root of horizontal permeability (see **Equation 5.1**). As the horizontal permeability is decreased, the capillary pressure will increase, thus less oil will be recovered. However, the upper limit improvement is higher for the case 2. It indicates that lowering IFT will give more significant effect if the capillary pressure of the system is originally high.

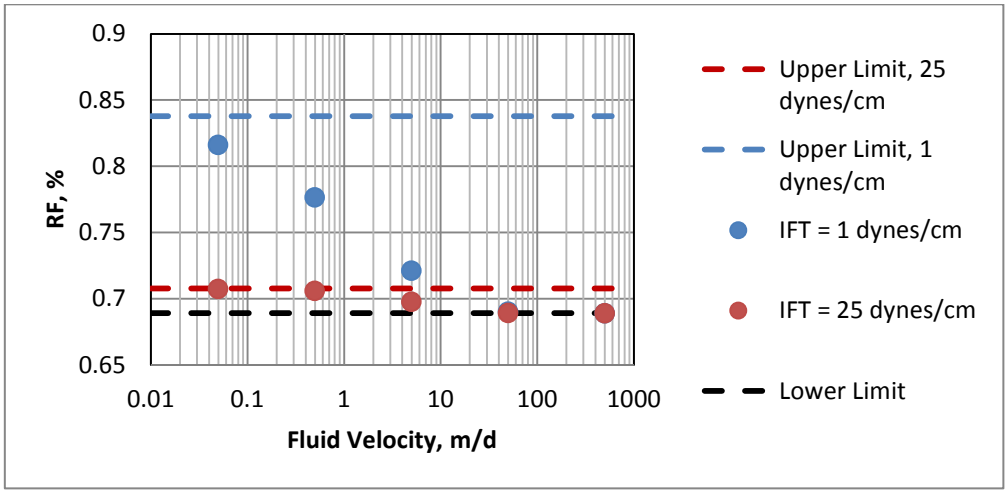

Figure 5.10 Simulation results from the case 2.

Table 5.5 Observations from the case 2 and the base case.

Results	Case 2, k_h = 250 md	Base Case, k_h = 1000 md
Critical Velocity, m/day	~20	~20
Upper Limit (IFT = 25 dynes/cm), %	71	73
Upper Limit (IFT = 1 dynes/cm), %	84	85
Upper Limit Improvement, %	18	16

5.5.3 Case 3: Effect of Oil Density

The simulation results from case 3 are presented in **Figure 5.11**. In this case, the oil density was varied while the water density was kept the same as the base case. The density difference is 150 kg/m3, which is 37.5% of the density difference in the base case. The main observations from this case are summarized in **Table 5.6**. For comparison, the observations from the base case simulations are also presented in the same table.

The critical velocity is estimated to be 8 m/day or lower, which is approximately 40% of the critical velocity given by the base case. This change is at the same order of magnitude as the

change of the density difference (37.5%). These results demonstrate that the critical velocity will decrease by a given factor when the density difference is decreased by the same factor.

The upper limits for high and low IFT are 70 and 83%, respectively. Both of those limits are slightly lower than those given by the base case. It occurs because density difference is the driving force in gravity segregation. As the driving force is decreased, the magnitude of gravity segregation will also decrease, thus less oil will be recovered. However, the upper limit improvement is higher for the case 3. It demonstrates that lowering IFT will give more significant effect when the driving force of gravity segregation is originally low.

Despite the oil density was varied from very low (600 kg/m^3) to very high density (850 kg/m^3), the effect on segregation is small. It indicates that the magnitude of gravity segregation is relatively insensitive to the magnitude of the density difference for the range of densities normally encountered in actual oil production operations.

It is worth to mention that the oil viscosities were kept constant at 0.5 cp for those runs, although physically, a change in oil density should be accompanied by a change in viscosity. The reason for not changing the oil viscosity when the density was changed was simply because the objective of these simulations was to isolate the influence of the density difference on gravity segregation.

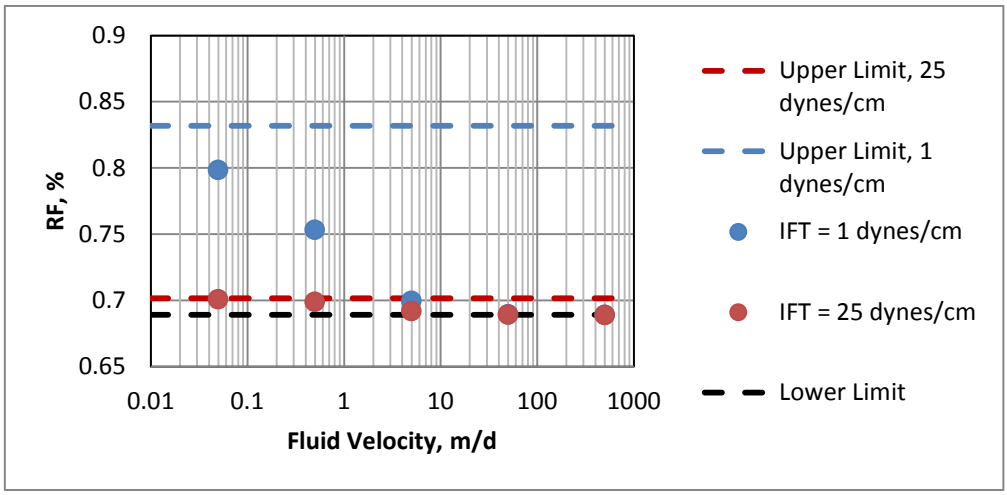

Figure 5.11 Simulation results from the case 3.

Table 5.6 Observations from the case 3 and the base case.

Results	Case 3, ρ_o = 850 kg/m3	Base Case, ρ_o = 600 md
Critical Velocity, m/day	~8	~20
VE Limit (IFT = 25 dynes/cm), %	70	73
VE Limit (IFT = 1 dynes/cm), %	83	85
VE Limit Improvement, %	18.5	16

5.5.4 Case 4: Effect of Model Thickness

In the case 4, the model thickness is ten times larger than that in the base case. The simulation results are presented in **Figure 5.12**. The main observations from this figure, along with the observations from the base case, are summarized in **Table 5.7**.

The critical velocity is estimated to be 5 m/day, which is ten times lower than that given by the base case. These results clearly demonstrate that an increase in the model thickness by a given factor will decrease the critical velocity by the same factor. It occurs because the oil phase has to travel in a longer vertical distance in order to reach the top of the model.

The upper limit increases from 83% to 87% when the water-oil IFT is decreased from 25 to 1 dynes/cm. Both of those upper limits are higher than those given by the base case simulations. It occurs because the hydrostatic pressure of the water phase is higher in the thicker model. Therefore, the water phase has higher potential to move downwards and displace the oil phase to the top of the model. When the potential of having gravity segregation is already high, lowering IFT will only give small oil recovery improvement. It is shown by the upper limit which increases only by 5% when the IFT is decreased from 25 to 1 dynes/cm. It is much less than the upper limit improvement given by the base case (thin model), 16%.

Table 5.7 Observations from the case 4 and the base case

Results	Case 4, H = 20 m	Base Case, H = 2 m
Critical Velocity, m/day	~5	~50
VE Limit (IFT = 25 dynes/cm), %	83	73
VE Limit (IFT = 1 dynes/cm), %	87	85
VE Limit Improvement, %	5	16

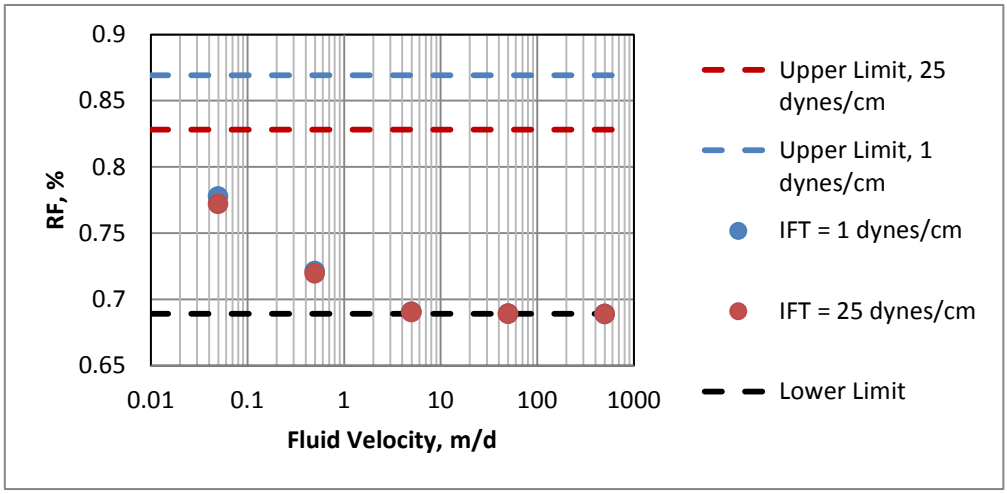

Figure 5.12 Simulation results from the case 4.

5.5.5 A Correlation for Predicting the Critical Velocity

Critical velocity represents a condition when the gravity forces start to overcome the viscous forces, thus gravity segregation occurs. The gravity forces are driven by the density difference, while pressure gradient is the driving mechanism in the viscous forces. A correlation between the critical velocity and these two parameters (density difference and pressure gradient) was established. The correlation is based upon the simulation results previously discussed. Vertical permeability and thickness would also be taken into account in the correlation since they affect the critical velocity (see **Section 5.5.1** and **Section 5.5.4**).

An attempt was made to correlate the oil recoveries with viscous-gravity forces ratio (R_{vg}) in the form of the following equation.

$$R_{vg} = \frac{\frac{\Delta p}{L} \times k_h}{\Delta \rho \times g \times k_v}\left(\frac{h}{L}\right) \tag{5.2}$$

Where $\Delta p/L$ = pressure gradient, $\Delta \rho$ = density difference, g = gravitational acceleration, k_v = vertical permeability, k_h = horizontal permeability, h = thickness, and L = length. This dimensionless number was chosen since it contains all the pertinent parameters. It should be noted that **Equation 5.2** is slightly different from the viscous-gravity forces ratio proposed by Stalkup (1983) in which h is the denominator and L is the numerator. Stalkup's equation is applicable for evaluating gravity segregation at the displacement front, whereas this study

focuses on gravity segregation that takes place behind the displacement front. The required Δp data from all of the simulations carried out in this study are presented in **Appendix C**.

Figure 5.13 through **Figure 5.16** show oil recovery factor as a function of R_{vg} for all of the cases. It can be seen that in each case, the curves start to deviate from the lower plateau when R_{vg} is approximately one. It indicates that the gravity segregation will occur when the gravity forces are higher than the viscous forces.

These results demonstrate that viscous-gravity forces ratio can be used as an indicator to determine under which condition gravity segregation occurs. For a system with a given water-oil density difference, horizontal and vertical permeability, and geometry (length and height), one can use this correlation to predict the required pressure difference or velocity for gravity segregation to occur.

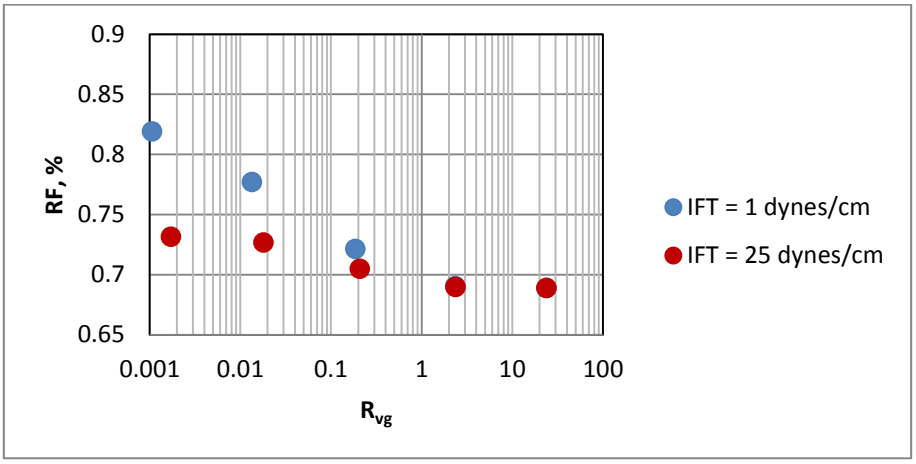

Figure 5.13 Oil recovery factor as a function of R_{vg} for the base case.

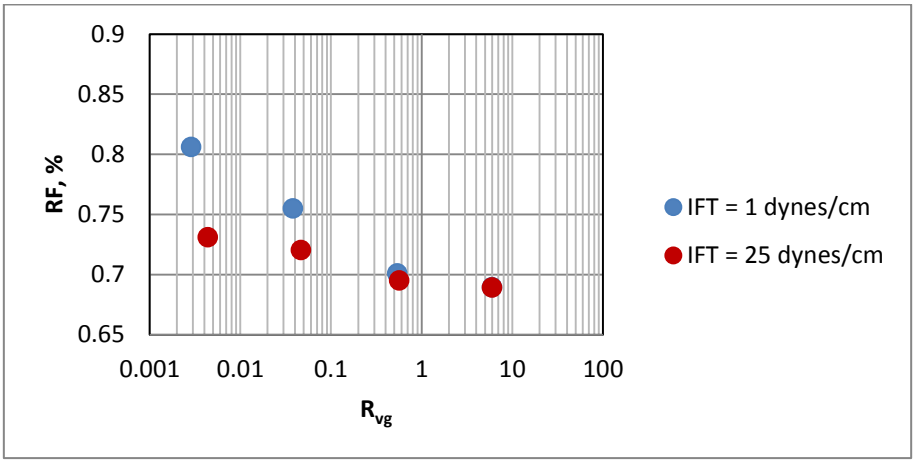

Figure 5.14 Oil recovery factor as a function of R_{vg} for the case 1.

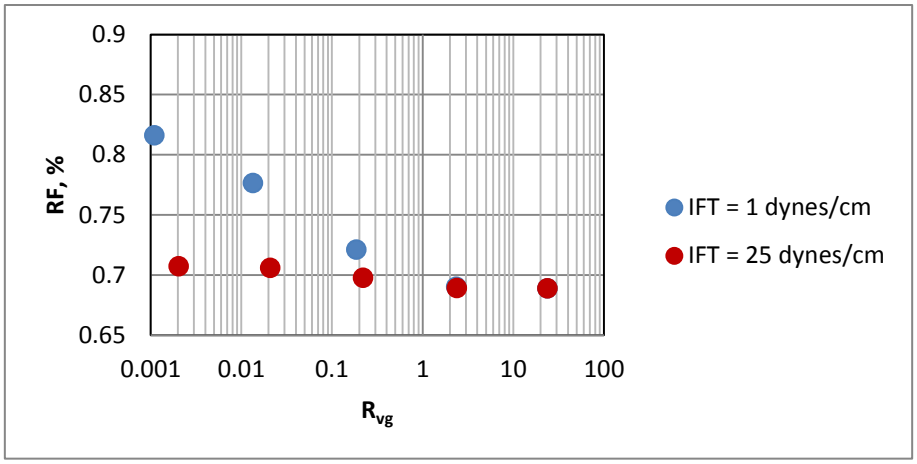

Figure 5.15 Oil recovery factor as a function of R_{vg} for the case 2.

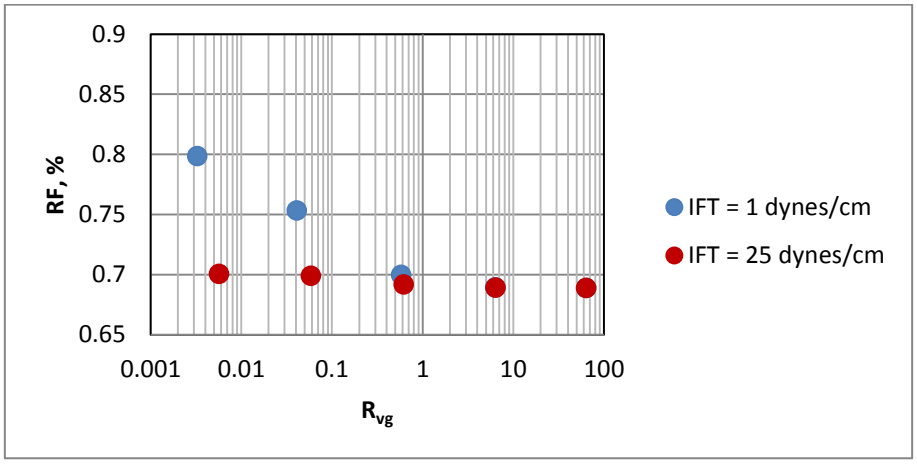

Figure 5.16 Oil recovery factor as a function of R_{vg} for the case 3.

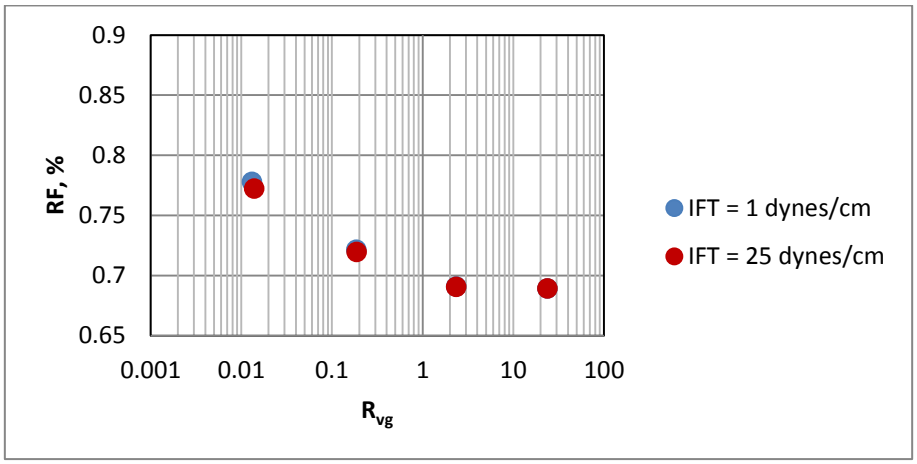

Figure 5.17 Oil recovery factor as a function of R_{vg} for the case 4.

5.5.6 A Correlation for Predicting the VE Limit

The upper limit represents the maximum oil recovery given by the gravity segregation mechanism. In the previous section, it was shown that the upper limit increases with decreasing water-oil IFT, increasing density difference, increasing the model thickness, and increasing horizontal permeability. Here, attempts were made to correlate the upper limits with several possible dimensionless numbers which combine all of those pertinent parameters.

From several possible combinations, it was found that the most satisfactory correlation is given by a plot of the upper limits versus log Bond number (N_B). The Bond number is defined as follow:

$$N_B = \frac{\Delta\rho \times g \times H \times \sqrt{k_h}}{IFT} \tag{5.3}$$

Where $\Delta\rho$ = density difference, g = gravitational acceleration, H = model thickness, k_h = horizontal permeability, and IFT = water-oil interfacial tension. This correlation combines the micro-scale parameter and macro-scale parameter (H). Two additional runs were made with the data set as presented in **Table 5.8**. The plot of upper limits as a function of log N_B from all of the one-dimensional simulations carried out in this study, including the two additional runs, is shown in **Figure 5.18**. It can be seen that there is a lower plateau at low N_B and an upper plateau at high N_B. Between those plateaus, VE limit increases with increasing N_B. N_B equals to one seems to be the inflection point where the curve changes from being concave upwards (positive curvature) to concave downwards (negative curvature).

Table 5.8 Data set for additional run #1 and #2.

Parameter	Additional Run #1	Additional Run #2
ρ_w, kg/m^3	1000	1000
ρ_o, kg/m^3	600	980
g, m/s^2	9.8	9.8
k_h	1E-12	1E-12
H	2	2
IFT	0.008	0.025
N_B	0.98	0.01568

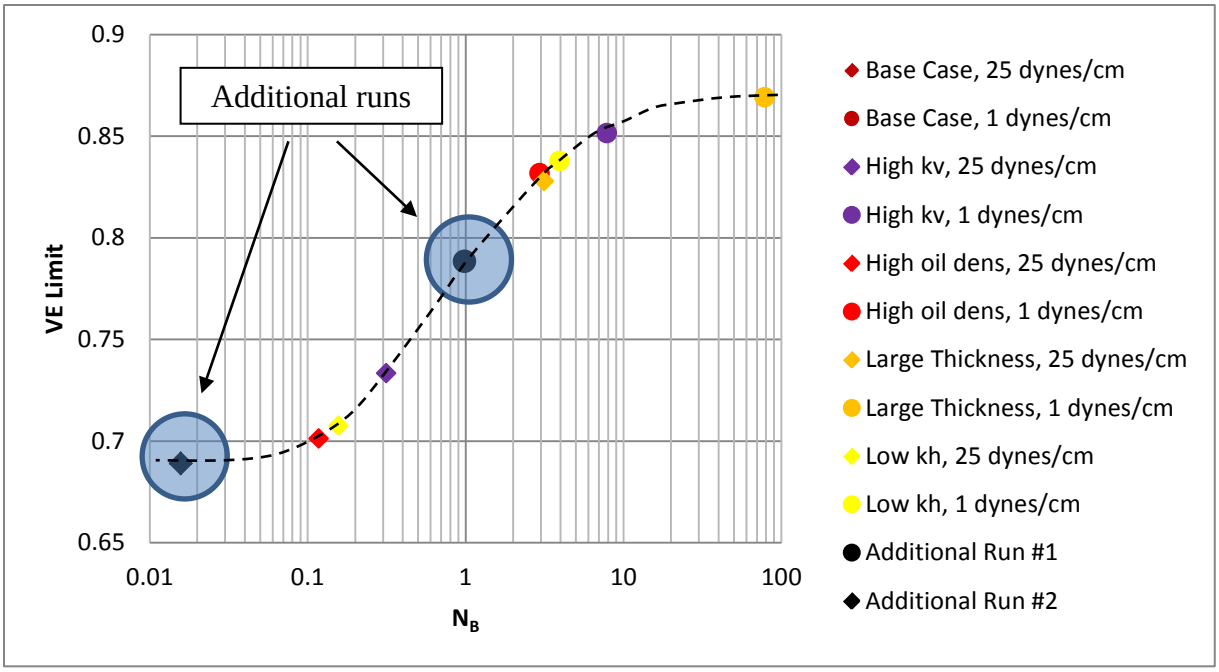

Figure 5.18 VE limit as a function of N_B.

If the Bond numbers are plotted against S_{or}, as shown in **Figure 5.19**, the shape of the curve would resemble the CDC (see **Figure 3.4**). These results demonstrate that the Bond number has to be increased above a critical value in order to decrease the residual oil saturation. In this simulation model, this critical Bond number is approximately around 0.07.

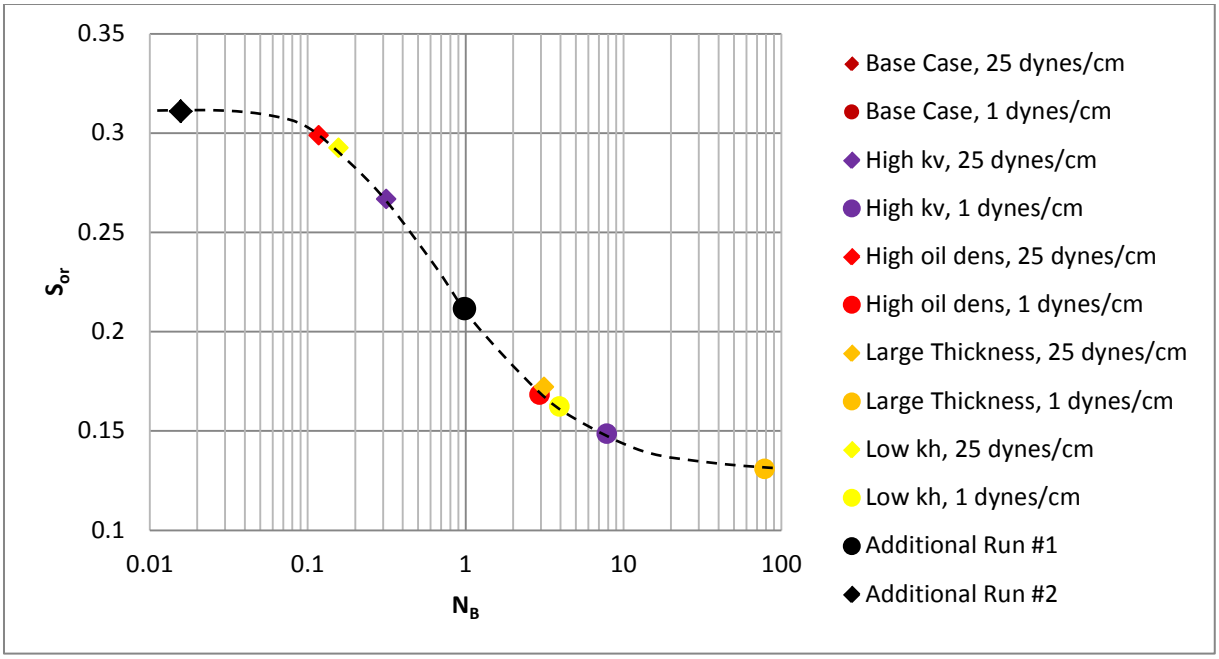

Figure 5.19 Residual oil saturation as a function of N_B.

6 CONCLUSIONS AND RECOMMENDATIONS

6.1 Conclusions

This simulation study enabled the following conclusions to be made.

1. Gravity segregation behind the displacement front gives positive effect on oil recovery by accumulating the oil phase at the top of the model, thus improving the effective horizontal oil mobility. In an ideal model, the oil recovery could be 16% higher than that would be predicted if gravity segregation was ignored.
2. Simulations in various models indicate that reducing IFT will increase the degree of gravity segregation, thus improving the oil recovery. The effect of reducing IFT was found to be more significant in a thin model with low horizontal permeability, and high density difference. However, the degree of gravity segregation is relatively insensitive to the magnitude of the oil densities normally encountered in actual oil production operations.
3. There is a critical velocity above which gravity segregation will not occur. Reducing the velocity below the critical value will increase the degree of gravity segregation until an equilibrium condition is reached.
4. The critical velocity was found to increase with increasing vertical permeability, increasing density difference, and decreasing the model thickness.
5. The oil recovery at the equilibrium condition represents the maximum oil recovery given by gravity segregation mechanism. It can be predicted by using one-dimensional simulation with vertical equilibrium (VE) upscaled relative permeability curves.
6. Gravity segregation was found to occur when the dimensionless viscous-gravity forces ratio (R_{vg}) is around 1. This correlation can be used to estimate the required pressure difference or injection velocity for the gravity segregation to occur.
7. A correlation between residual oil saturation and Bond number (N_B) has a similar shape as the Capillary Desaturation Curve (CDC). There is a critical Bond number where gravity forces starts to overcome the capillary forces and decrease the residual oil saturation.
8. Both the R_{vg} and N_B correlations were derived using an ideal homogenous model. It may not be applicable to heterogeneous reservoirs.

6.2 Recommendations for Further Work

Although this master thesis is considered as completed, further work is absolutely necessary to fully understand the effect of gravity segregation on oil recovery, and how reservoir and fluid properties affect the mechanism.

The reservoir models used in this work are homogenous, whereas rocks in the field are rarely homogenous. Therefore, it is recommended to investigate the effect of reservoir heterogeneity. In addition to that, it is also recommended to perform the same study for different wettability preferences (i.e. water wet and oil wet) to investigate how wettability affects the gravity segregation mechanism.

In this study, the surfactant solution was injected continuously from the beginning of the displacement process. In order to make it more realistic, one can make simulations with the surfactant slug being injected after several PV of water injection. Several numerical difficulties were also encountered when running the simulations at extremely low velocities, thus finding a way (probably by making some changes in TUNING keyword) to solve this problem could also be a good improvement for further work.

REFERENCES

ECLIPSE Technical Description. (2009). Schlumberger.

(2011, May). Retrieved from U.S. Energy Information Administration: http://www.eia.gov

Agbalaka, C. D. (2008). The Effect of Wettability on Oil Recovery: A Review. *SPE 114496*.

Anderson, W. (1986). Wettability Literature Survey - Part 2: Wettability Measurement. *JPT*, 1246-1262.

Anderson, W. (December 1987c). Wettability Literature Survey – Part 6: The Effects of Wettability on Waterflooding. *JPT*, 1605-1622.

Anderson, W. (November 1987b). Wettability Literature Survey – Part 5: The Effects of Wettability on Relative Permeability. *JPT*, 1453-1468.

Anderson, W. (October 1987a). Wettability Literature Survey – Part 4: Effects of Wettability on Capillary Pressure. *JPT*, 1238-1300.

Bardon, C. L. (October 1980). Influence of Very Low Interfacial Tensions on Relative Permeability. *SPE Journal*, 391-401.

Batychy, J. M. (1978). Low Interfacial Tension Displacement Studies. *Petroleum Society of CIM 78-29-26*.

Behbahani, H. B. (2004). Analysis of Imbibition in Mixed-Wet Rocks Using Pore-Scale Modeling. *SPE 90132*.

Cosentino, L. (2001). Integrated Reservoir Studies. Paris: Editions Technip.

Craft, B. H. (1991). Applied Petroleum Reservoir Engineering. Englewood Cliffs, NJ: Prentice Hall.

Donaldson, E. T. (1971). Microscopic Observations of Oil Displacement in Water-Wet and Oil-Wet Systems. *SPE 3555*.

Dong, H. H. (2006). The Effect of Wettability on Oil Recovery of Alkaline/Surfactant/Polymer Flooding. *SPE 102564*.

Dyke, K. (1997). Fundamentals of Petroleum. Austin, Texas: Petroleum Extension Service.

Garnes, J. M. (1990). Capillary Number Relations for Some North Sea Reservoir Sandstones. *SPE/DOE 20264*.

Gilliland, H. C. (1976). A Pilot Test of Surfactant Flooding in the Big Muddy Field. *SPE 5891*.

Green, D. W. (1998). Enhanced Oil Recovery. Richardson, Texas: SPE.

Healy, R. R. (April 1977). Immiscible Microemulsion Flooding. *SPE Journal*, 129-139.

Healy, R. R. (June 1976). Multiphase Microemulsion Systems. *SPE Journal*, 147-160.

Hornof, V. M. (1987). Gravity Effects in the Displacement of Oil by Surfactant Solutions. *SPE 13573*.

Hornof, V. M. (1987). Gravity Effects in the Displacement of Oil by Surfactant Solutions. *SPE 13573*.

Kolnes, J. (1992). Surfactant Flooding Displacement Mechanisms. In S. K. Skjæveland, *SPOR Monograph: Recent Advances in Improved Oil Recovery Methods for North Sea Sandstone Reservoirs* (pp. 239-243). Stavanger: NPD.

Lake, L. (1989). *Enhanced Oil Recovery*. Englewood Cliffs, NJ: Prentice Hall Inc.

Lohne, A. V. (2007). *Flow 2D User's Manual*. Stavanger: IRIS.

Melrose, J. B. (October-December 1974). Role of Capillary Forces in Determining Microscopic Displacement Efficiency for Oil Recovery by Waterflooding. *JCPT*, 54-62.

Morrow, N. (July-September 1979). Interplay of Capillary, Viscous, and Buoyancy Forces in the Mobilization of Residual Oil. *JCPT*, 35-46.

Morrow, N. (July-September 1979). Interplay of Capillary, Viscous, and Buoyancy Forces in the Mobilization of Residual Oil. *JCPT*, 35-46.

Morrow, N. S. (1981). Effect of Viscous and Buoyancy Forces on Non-Wetting Phase Trapping in Porous Media. In O. Shah, *Surface Phenomena in Enhanced Oil Recovery* (pp. 387-411). New York: Plenum Press.

Ottewill, R. (1984). Surfactants. San Fransisco: Academic Press.

Rao, D. G. (June 1992). The Influence of Reservori Wettability on Waterflood and Miscible Flood Performance. *JCPT*, 47-55.

Raza, S. T. (April 1968). Wettability of Reservoir Rocks and Its Evaluation. *Prod. Monthly*, 2-7.

Salathiel, R. (October 1973). Oil Recovery by Surface Film Drainage in Mixed Wettability Rocks. *JPT*, 1216-1224.

Schester, D. Z. (1991). Capillary Imbibition and Gravity Segregation in Low IFT Systems. *SPE 22594*.

Wood, A. W. (1991). Determining Effective Residual Oil Saturation for Mixed Wettability Reservoirs: Endicott Field, Alaska. *SPE 22903*.

APPENDICES

A Eclipse Input Data for Base Case

```
-------
RUNSPEC
-------
TITLE
  BASE CASE MODEL
DIMENS
  100  1  20  /
NONNC
OIL
WATER
SURFACT
METRIC
TABDIMS
  2  1  100  20  1  /
ENDSCALE
  /
WELLDIMS
  2  50  1  2  /
START
  7  MAY  2011  /
NSTACK
  50  /
--NOSIM


----
GRID
----
INIT
DXV
  100*5  /
DYV
  1*5  /
DZ
```

```
  2000*0.1  /
PERMX
  2000*1000  /
PERMY
  2000*1000  /
PERMZ
  2000*250  /
PORO
  2000*0.25  /
TOPS
  100*2500  /
JFUNC
--DYNE.PER.CM
  WATER  25  /
RPTGRID
  /

-----
PROPS
-----
SWFN
--SW              KRW           J
0.148000        0.00000000    200.0000
0.149590        0.00000001    23.83791
0.153375        0.00000002    6.147762
0.160945        0.00000004    2.258275
0.168515        0.00000009    1.309519
0.176085        0.00000021    0.888995
0.183655        0.00000036    0.653511
0.191225        0.00000054    0.503619
0.198795        0.00000081    0.400102
0.206365        0.00000121    0.324441
0.213935        0.00000176    0.266779
0.221505        0.00000255    0.221397
0.229075        0.00000369    0.184753
```

0.244215	0.00000755	0.129192
0.259355	0.00001484	0.088996
0.274495	0.00002852	0.058471
0.289635	0.00005262	0.034401
0.304775	0.00009491	0.014834
0.335055	0.00027820	-0.01540
0.365335	0.00071893	-0.03820
0.395615	0.00165294	-0.05664
0.425895	0.00349981	-0.07248
0.447636	0.00578936	-0.08290
0.469377	0.00923191	-0.09289
0.491118	0.01434285	-0.10273
0.512859	0.02171011	-0.11267
0.534600	0.03157445	-0.12296
0.556341	0.04460744	-0.13386
0.578082	0.06139899	-0.14570
0.599823	0.08195209	-0.15884
0.621564	0.10528319	-0.17378
0.643305	0.13247879	-0.19114
0.665046	0.16376902	-0.21182
0.686787	0.19981156	-0.23710
0.708528	0.24134976	-0.26888
0.730269	0.28903769	-0.31019
0.752010	0.34284329	-0.36598
0.773751	0.40138466	-0.44506
0.795492	0.46591559	-0.56445
0.817233	0.53621018	-0.76117
0.838974	0.60968389	-1.13094
0.860716	0.68594618	-2.00247
0.868286	0.71379943	-2.62999
0.875856	0.74223685	-3.68938
0.890996	0.79588497	-10.9333
0.898566	0.82414609	-34.9465
0.902351	0.83865077	-132.058
0.903108	0.84158220	-218.707

0.903865 0.84452387 -470.499
0.905000 0.84747583 -600.000
/
0.148000 0.00000000 200.0000
0.149590 0.00000001 23.83791
0.153375 0.00000002 6.147762
0.160945 0.00000004 2.258275
0.168515 0.00000009 1.309519
0.176085 0.00000021 0.888995
0.183655 0.00000036 0.653511
0.191225 0.00000054 0.503619
0.198795 0.00000081 0.400102
0.206365 0.00000121 0.324441
0.213935 0.00000176 0.266779
0.221505 0.00000255 0.221397
0.229075 0.00000369 0.184753
0.244215 0.00000755 0.129192
0.259355 0.00001484 0.088996
0.274495 0.00002852 0.058471
0.289635 0.00005262 0.034401
0.304775 0.00009491 0.014834
0.335055 0.00027820 -0.01540
0.365335 0.00071893 -0.03820
0.395615 0.00165294 -0.05664
0.425895 0.00349981 -0.07248
0.447636 0.00578936 -0.08290
0.469377 0.00923191 -0.09289
0.491118 0.01434285 -0.10273
0.512859 0.02171011 -0.11267
0.534600 0.03157445 -0.12296
0.556341 0.04460744 -0.13386
0.578082 0.06139899 -0.14570
0.599823 0.08195209 -0.15884
0.621564 0.10528319 -0.17378
0.643305 0.13247879 -0.19114

0.665046 0.16376902 -0.21182
0.686787 0.19981156 -0.23710
0.708528 0.24134976 -0.26888
0.730269 0.28903769 -0.31019
0.752010 0.34284329 -0.36598
0.773751 0.40138466 -0.44506
0.795492 0.46591559 -0.56445
0.817233 0.53621018 -0.76117
0.838974 0.60968389 -1.13094
0.860716 0.68594618 -2.00247
0.868286 0.71379943 -2.62999
0.875856 0.74223685 -3.68938
0.890996 0.79588497 -10.9333
0.898566 0.82414609 -34.9465
0.902351 0.83865077 -132.058
0.903108 0.84158220 -218.707
0.903865 0.84452387 -470.499
0.905000 0.84747583 -600.000
/
SOF2
--SO KRO
0.09500 0.00000000
0.12528 0.00000077
0.15556 0.00000491
0.18584 0.00002617
0.21612 0.00011603
0.2464 0.00042824
0.27668 0.00131584
0.30696 0.00336597
0.33724 0.00716820
0.36752 0.01275780
0.3978 0.02070515
0.42808 0.03237853
0.45836 0.04878788
0.48864 0.07083417

0.51892 0.09909457
0.5492 0.13357739
0.57948 0.17349708
0.60976 0.21713381
0.64004 0.26475376
0.67032 0.32144566
0.7006 0.38839826
0.73088 0.46703697
0.76116 0.55889411
0.79144 0.66559810
0.82172 0.78885812
0.8520 0.93044349
/
0.09500 0.00000000
0.12528 0.00000077
0.15556 0.00000491
0.18584 0.00002617
0.21612 0.00011603
0.2464 0.00042824
0.27668 0.00131584
0.30696 0.00336597
0.33724 0.00716820
0.36752 0.01275780
0.3978 0.02070515
0.42808 0.03237853
0.45836 0.04878788
0.48864 0.07083417
0.51892 0.09909457
0.5492 0.13357739
0.57948 0.17349708
0.60976 0.21713381
0.64004 0.26475376
0.67032 0.32144566
0.7006 0.38839826
0.73088 0.46703697

```
0.76116          0.55889411
0.79144          0.66559810
0.82172          0.78885812
0.8520           0.93044349
/
PVTW
--P  FVF  COMP  VISC  VISCOSIBILITY
 250  1  0  0.3  0  /
PVDO
--P  FVF  VISC
 250  1.0000  0.5
 50000  0.9999  0.5  /
ROCK
--P  COMP
 250  1E-9  /
DENSITY
--OIL  WATER  GAS
 600  1000  10  /
SURFVISC
--CONC  VISC
 0   0.3
 10  0.3  /
SURFST
--CONC  IFT.NEWTON.PER.M
 0.0  0.025
 0.5  0.001
 1.5  0.0001
 3.0  0.00001
 6.0  0.000001
 10   0.000001  /
SURFCAPD
--LOGNC  1=MISC  0=IMMISC
 -9.0  0.0
 -4.5  0.0
 -2.0  1.0
```

```
  10   1.0  /
 -9.0  0.0
 -4.5  0.0
 -2.0  1.0
  10   1.0  /
RPTPROPS
 'SURFVISC'  /

-------
REGIONS
-------
SATNUM
 2000*1  /
SURFNUM
 2000*2  /
RPTREGS
 /
--------
SOLUTION
--------
EQUIL
--DEPTH  BHP  WOC  PC
 2500  250  2510  5  /
RPTSOL
 'PRES'  'SOIL'  'SWAT'  'RESTART=1'  'SURFBLK'  'FIPSURF=2'  /

-------
SUMMARY
-------
FOE
--RECOVERY FACTOR
FOPR
--FIELD.OIL.PROD.RATE
FOPT
--FIELD.OIL.PROD.TOTAL
```

```
FOIP
--FIELD.OIL.IN.PLACE
FOSAT
--FIELD.OIL.SATURATION
FWIR
--FIELD.WATER.INJ.RATE
FWIT
--FIELD.WATER.INJ.TOTAL
FWPR
--FIELD.WATER.PROD.RATE
FWCT
--FIELD.WATER.CUT
FWIP
--FIELD.WATER.IN.PLACE
FLPR
--FIELD.LIQUID.PROD.RATE
FVPR
--RES.VOL.PROD.RATE
FVPT
--RES.VOL.PROD.TOTAL
FVIR
--RES.VOL.INJ.RATE
FVIT
--RES.VOL.INJ.TOTAL
WBHP
 /
EXCEL
RUNSUM


--------
SCHEDULE
--------
RPTSCHED
 'PRES' 'SOIL' 'SWAT' 'RESTART=2' 'FIP=2' 'WELLS=1' 'SUMMARY=2' 'CPU=2'
'SURFBLK' 'FIPSURF=2' /
```

```
WELSPECS
--WELL  GROUP  I  J  DEPTH  PHASE
 'PRO'  'G'  100  1  2500  'OIL'  /
 'INJ'  'G'   1  1  2500  'WAT'  /
 /
COMPDAT
--WELL  I  J  K1  K2  OPEN.CLOSE  1*  WELL.CON.FACTOR  RW
 'PRO'  100  1  1  20  'OPEN'  1*  34.108  /
 'INJ'   1  1  1  20  'OPEN'  1*  34.108  /
 /
WCONPROD
--WELL  OPEN.CLOSE  CONTROL  4*  RESV  BHP.LOWER.LIMIT
 'PRO'  'OPEN'  'BHP'  5*  200  /
 /
WCONINJE
--WELL  PHASE  OPEN.CLOSE  CONTROL  RATE  RESV  BHP.UPPER.LIMIT
 'INJ'  'WAT'  'OPEN'  'RESV'  1*  5  50000  /
 /
WSURFACT
--WELL  CONC
 'INJ'  0  /
 /
TUNING
 0.001  3  0.00001  1*  1.5  /
 1*  1E-5  1*  1E-7  /
 100  1*  100  1*  100  /
TSTEP
 1250  /
END
```

B Flow2D Upscaling Input Data for Base Case

```
runsect
*IDENTIFICATION OF THE RUN (CASE DESCRIPTION).
------------------------------------------------------------------------
------------------------------------------------------------------------
title
  'Homogeneous model: 500m×2m'  /
ruNflags
  2  1  1  0  1  /
rateflag
  0  /
sourcedim
  100  20  1  1  0  0  /
phases
  1  1  0  /
nrock
  1  /
nstack
  30  /
pause
  1  /

------------------------------------------------------------------------
gridsect
------------------------------------------------------------------------
orientation
  90  0  /
permx
  1  /  Darcy
permy
  0.25  /
poro
  15000*0.25  /
dx
  100*500  /  cm
```

```
dy
  20*10  /  cm

---------------------------------------------------------------------
propsect
---------------------------------------------------------------------
density
  0.6  1  0.010  /  (g/ml)
ift
  25  1  /  mN/m=dynes/cm
viscosity
  0.5  0.3  0.0289  /  o-w-g
jscale
  1  /
krtab1
  1  1  2  3  1  /  rock 1
include "incl/relp_mixed-wet_1.txt" /
  /
pctab1
  1  1  3  /
include "incl/Pc_imb_mixed-wet_1.txt" /
  /
swco
  1  1  1  /

---------------------------------------------------------------------
compsect
---------------------------------------------------------------------
PcwLIST
  40  2  2  /
  -2.5  -1.25  /
  1.25  2.5  /
newttol
  500  0.01  0.00001  /
dtcalc
```

```
  0.2  0.0001  1.1  0.75  1  0  0  /
dttol
  1e-10  0.0001  2  3  200  /
lintol
  500  1e-10  /
confact
  1e6  10000  1  1  /
solver
  1  2  /
upstream
  1  /
end
```

C Production and Injection Well Bottomhole Pressure for All 1D Simulations

k_v = 250 md, k_h = 1000 md, ρ_o = 600 kg/m^3, H = 2 m

IFT = 25 dynes/cm			IFT = 1 dynes/cm		
RF, %	WBHP-I	WBHP-P	RF, %	WBHP-P	WBHP-I
0.73154	202.1	200	0.81905	201.3	200
0.72681	222	200	0.77695	216.4	200
0.70495	455	200	0.72128	428	200
0.68982	3099	200	0.6906	3077.4	200
0.68902	29415.3	200	0.68902	29414.9	200

k_v = 1000 md, k_h = 1000 md, ρ_o = 600 kg/m^3, H = 2 m

IFT = 25 dynes/cm			IFT = 1 dynes/cm		
RF, %	WBHP-I	WBHP-P	RF, %	WBHP-P	WBHP-I
0.73202	202.1	200	0.83557	201.3	200
0.73092	221.4	200	0.80598	214.1	200
0.72027	428.5	200	0.75491	385.7	200
0.69514	2958.8	200	0.70089	2832.4	200
0.68911	29385.8	200	0.6893	29329	200

k_v = 250 md, k_h = 250 md, ρ_o = 600 kg/m^3, H = 2 m

IFT = 25 dynes/cm			IFT = 1 dynes/cm		
RF, %	WBHP-I	WBHP-P	RF, %	WBHP-P	WBHP-I
0.70729	210	200	0.8162	205.4	200
0.7059	301.8	200	0.77656	265.7	200
0.69771	1279.5	200	0.72103	1112.6	200
0.68927	11828.7	200	0.69027	11716.5	200
0.68883	116974.6	200	0.68883	116972.6	200

k_v = 250 md, k_h = 1000 md, ρ_o = 850 kg/m^3, H = 2 m

IFT = 25 dynes/cm			IFT = 1 dynes/cm		
RF, %	WBHP-I	WBHP-P	RF, %	WBHP-P	WBHP-I
0.70072	202.6	200	0.79849	201.5	200
0.69893	226.9	200	0.75324	218.8	200
0.69185	484.3	200	0.6997	465.7	200
0.68917	3118.2	200	0.68938	3112	200
0.68902	29415.7	200	0.68902	29415.7	200

k_v = 250 md, k_h = 1000 md, ρ_o = 600 kg/m^3, H = 20 m

IFT = 25 dynes/cm			IFT = 1 dynes/cm		
RF, %	WBHP-I	WBHP-P	RF, %	WBHP-P	WBHP-I
0.77216	201.7	200	0.77777	201.6	200
0.71957	223	200	0.72145	222.8	200
0.69051	487.9	200	0.69065	487.6	200
0.68916	3118.7	200	0.68916	3118.8	200
0.68901	29416.5	200	0.68901	29416.5	200